CODED CONTINUOUS PHASE MODULATION FOR TACTICAL COMMUNICATIONS

A Thesis

by

Mahsa Foruhandeh

Submitted to the
Graduate School of Sciences and Engineering
In Partial Fulfillment of the Requirements for
the Degree of

Master of Science

in the
Department of Electrical and Electronics Engineering

Özyeğin University
August 2014

CODED CONTINUOUS PHASE MODULATION FOR TACTICAL COMMUNICATIONS

Approved by:

Professor Murat Uysal, Advisor
Department of Electrical and Electronics Engineering
Özyeğin University

Professor Cenk Demiroğlu
Department of Electrical and Electronics Engineering
Özyeğin University

Professor Haci Ilhan
Department of Electrical and Electronics Engineering
Yildiz Technical University

Date Approved: 14 August 2014

To the memory of my beloved father.

ABSTRACT

Satisfying the various demands of tactical transceivers is one the common challenges in military communications. Different modulation, coding and spread spectrum techniques are needed to meet these requirements. Although FSK is the most popular modulation technique used for tactical waveforms and frequently employed in military walkie-talkies, Continuous Phase Modulation (CPM) is superior to this conventional method due to its spectral efficiency feature. High spectral efficiency and constant envelope are the specifications that make this modulation technique attractive for tactical waveforms. Serial concatenation of CPM with Low Density Parity Check Codes (LDPCs) provides a superior performance due to coding gains of this powerful code family. The choice of proper combination of LDPC and CPM is crucial to satisfy the targeted tactical waveform requirements of spectral efficiency, power efficiency and receiver complexity. In this thesis we address the problem of selecting the optimal transmission parameters in an LDPC-coded CPM system and investigating the performances under different jamming scenarios. The parameters are chosen to satisfy a given spectral efficiency subject to a constraint on the demodulator complexity. Specifically, we consider modulation index, alphabet size, pulse shape duration and code rate as transmission parameters. Utilizing a systematic search procedure, we identify the proper transmission parameters to achieve a targeted spectral efficiency and error rate. Thereafter, the selected schemes are tested under attack of different frequency jamming signals.

ÖZETÇE

Taktik alıcı-vericilerin eşitli gerekliliklerini yerine getirmek askeri haberleşmenin en yaygn sorunlarndan biridir. Farklı modülasyon, kodlama ve geniş spektrum teknikleri bu ihtiyaları karşılamalıdır. FSK, askeri telsiz ve taktiksel dalga formları iin en yaygın olarak kullanılan modülasyon tekniği olsada, devamlı faz modülasyonu (CPM) spektral verimlilik özelliğinden dolayı bu geleneksel teknikten ok daha üstündür. Bu modülasyon tekniğini taktiksel dalga formları iin ekici kılan özellik yüksek spektral verimlilik ve sabit kılıf tanımlarıdır. CPM ve düşük yoğunluk parite kontrol kodlarının seri bağlanması, kodlama verimliliğinden ötürü üstün bir performans sağlar. LDPC ve CPM uygun bir şekilde seilmesi; spektral verimlilik, gü verimliliği ve kompleks alıcı gereklilikleri asndan büyük bir önem taşır. Bu tez, LDPC kodlu CPM sisteminde optimal gönderme parametrelerini seerek, farklı bozucu sinyal durumları altında performans araştırması yapmak üzerine yazılmıştır. Parametreler kompleks demodülatör sınırlarına bağlı olarak verilen spektral verimliliğe uyumlu olarak seilmiştir. Özellikle, modülasyon ieriği, alfabe boyutu, titreşim şekli süresi ve kod oranı iletim parametreleri olarak kullanılmıştır. Sistematik arama prosedürü kullanılarak hedeflenen spektral verimlilik ve hata oranı elde edilmek üzere uygun iletim parametreleri belirlenmiştir. Belirlenen şemalar farklı frekans bozucu saldırılar altında test edilmiştir.

ACKNOWLEDGEMENTS

Primarily, I would like to convey my most genuine gratitude and appreciation for my adviser Professor Murat Uysal for the incessant encouragement, assistance and support in regards to my Master study and the research conducted, for his enduring patience, infinite motivation, fervor for the work I was doing, as well as his immeasurable knowledge. It was his aspiring guidance, invaluable constructive criticism and friendly advice that has helped me in the dimmest and most pessimistic times of conducting my research and writing this thesis, and I could not have envisioned having a finer mentor.

Furthermore, I would like to thank Professor Ibrahim Altunbaš for his support, astute comments, and valuable time invested in aiding me in successfully completing my thesis.

My most heartfelt appreciation also goes to my fellow group members, for their stimulating and energizing discussions, for all of their assistance and positive reinforcement They have been there for me throughout my many sleepless nights, and have played an unsurpassable role in both my private and professional life during my time at Özyeğin University.

I also would like to acknowledge the financial support from SAN-TEZ project (01553.STZ.2012-2) which made this work possible.

Last but not the least, I would like to thank my mom, my brother and sister in law for their timeless encouragement, undying affection and never-ending belief in me.

TABLE OF CONTENTS

LIST OF TABLES

LIST OF FIGURES

CHAPTER I

INTRODUCTION

Continuous phase modulation (CPM) has attractive features such as spectral efficiency and constant envelope making it attractive for tactical waveforms. There are a number of requirements in the design of these waveforms including energy efficiency in the transmitter amplifier to prolong battery life, minimization of out-of-band emissions to satisfy spectral masks and good error rate performance to achieve the desired quality of service as well as low receiver complexity. To satisfy these requirements, the use of continuous phase modulation (CPM) was proposed in [1, 2, 3, 4, 5] for tactical waveforms. CPM has a near constant envelope allowing its efficient use with nonlinear amplifiers. Furthermore, its superior spectral characteristics result in a high spectral efficiency. With such features, CPM is an ideal choice for tactical waveforms and currently adopted in the NATO VHF/UHF standard (STANAG) in AHWG/2 SC/6 [3].

Existing literature on tactical waveforms [6] have focused mostly on uncoded CPM with frequency hopping. To further boost the error rate performance of CPM, it can be used in conjunction with channel coding [2, 7, 8]. For example, the combination of CPM and convolutional coding has been proposed in [1, 3, 4, 5, 9, 10] for tactical use. Similarly, NATO STANAG standard defines two convolutional coded CPM waveforms. One waveform uses rectangular pulse shaping and modulation index 1/2 with a code rate of 2/3. The other waveform uses modulation index 1/8 and a code rate of 4/5. The first waveform exhibits good performance at low signal to noise ratios (SNRs), while the second waveform's spectral characteristics are particularly attractive. However the latter is designed to perform well in high SNRs. Reed-Solomon

codes [11], turbo codes [12] and LDPC [7, 8, 13] have been further proposed for combination with CPM. Among these, LDPC-coded CPM deserves particular attention with its superior error rate performance. It has been shown that a judiciously designed LDPC code can operate at 0.0045 dB within Shannon limit [14].

In this thesis, we address the problem of selecting the optimal transmission parameters to find the best trade-off between the power efficiency and spectral efficiency subject to a constraint on the demodulator complexity. After selecting the best scheme, we introduce different jamming signals that can attack the communication systems and we explore the selected scheme's performance in presence of these jamming signals in the system.

1.1 Continuous Phase Modulation

1.1.1 CPM Signal Model

Continuous Phase Modulation (CPM) is a kind of modulation in which the information is imbedded in phase. The basic idea behind this modulation is to avoid the abrupt jump of the carrier phase to zero at the beginning of each symbol period. With proper choice of parameters this modulation scheme can achieve higher bandwidth or power efficiency than that of other modulation schemes. Unlike the conventional FSK modulation signals, CPM signal is defined over the entire axis rather than just a symbol period. The CPM signal is defined as

$$s(t) = Acos(2\pi f_c t + \phi(t, a)), \quad -\infty < t < +\infty \tag{1}$$

where f_c is the carrier frequency and $\phi(t, a)$ denotes the time-varying phase. It can be noticed from (1) that the signal amplitude is constant and the message is inherent in the time varying phase. This phase term can be mathematically expressed as

$$\phi(t, a) = 2\pi h \sum_{i=-\infty}^{+\infty} a_i q(t - kT) \tag{2}$$

where h is the modulation index and α_i corresponds to i^{th} the data symbol which is drawn from the set $\{-(M-1), \ldots, -1, +1, \ldots, +(M-1)\}$ with M denoting the alphabet size. The modulation index h can take any real-valued number. But for practical implementation of the receiver (which will be described later) it is preferred to have a rational number. $q(t)$ is a continuous function and is called phase function in pulse shaping terminology. Phase function can be derived by taking integral over the pulse shaping function represented by $g(\tau)$ as

$$q(t) = \int_{-\infty}^{t} g(\tau) d\tau \tag{3}$$

where $g(\tau)$ is a smooth function over a finite time interval $0 \leq t \leq LT$. If $L \leq 1$, the pulse shaping signal remains within a symbol period and this leads to a full response pulse shape. Among different pulse shaping functions that can be used in CPM, rectangular pulse shape is a pulse with a length of L symbols and is defined as

$$g(t) = \begin{cases} \frac{1}{2LT} & 0 \leq t \leq LT \\ 0 & otherwise \end{cases} \tag{4}$$

This results in the following phase function

$$q(t) = \begin{cases} \int_0^t \frac{1}{2LT} dt & 0 < t < T \\ \int_0^T \frac{1}{2T} dt & t > T \end{cases} = \begin{cases} \frac{t}{2T} & 0 < t < T \\ \frac{1}{2} & t > T \end{cases} \tag{5}$$

Even when the pulse shaping function has a finite length, the phase function has an infinite length. This indicates that the CPM signals have infinite length memory [15]. Since the information in the phase of each modulated symbol contains the information from the current symbol along with the accumulated information of the previous symbols, the phase function can be rewritten as

$$\begin{aligned} &\phi(t, a) = 2\pi h \sum_{i=-\infty}^{k-L} a_i q(t - iT) + \\ &2\pi h \sum_{i=k-L+1}^{k-1} a_i q(t - iT) + 2\pi h a_n q(t - kT), \quad kT < t < (k+1)T \end{aligned} \tag{6}$$

In (6), the first term is the "cumulative phase" representing the constant part of the total carrier phase. The second term is called "correlative state vector" and represents the phase term corresponding to signal pulses that have not reached their final value. The third term is the phase contribution due to the most recent symbol which is called the "phase state" [15]. Eq.(6) can be summarized as

$$\phi(t,a) = \theta_k + 2\pi h \sum_{i=k-L+1}^{k} a_i q(t-iT) = \theta_k + \theta(t,a) \tag{7}$$

where θ_k is the cumulative phase and $\theta(t,a)$ is the instant phase. θ_k can be computed recursively via

$$\theta_{k+1} = \theta_k + \pi h a_{k-L+1} \tag{8}$$

By choosing h a rational number, in a way that $h = 2p/q$ while p and q have no common factors the phase transitions can be represented by a trellis. This trellis is used as a graphical tool in many demodulating algorithms which will be discussed later. CPM has several common special cases as well. For instance, if the length of the symbols (L) is set to 1, it will be referred to as continuous phase frequency-shift keying (CPFSK). There is also a special case of CPFSK which can be achieved if M is set to 2 and h is set to 0.5. This case is called Minimum Shift keying (MSK).

1.1.2 Demodulation Algorithms

There are many methods to demodulate the signals using the trellis diagram and state machine representation. Viterbi algorithm, BCJR algorithm, Log-MAP and Max-Log-MAP algorithms are the most common soft decisions methods that are used for CPM demodulation. Viterbi algorithm is a Maximum Likelihood demodulator that demodulates the signals based on the Euclidean distance of the transmitted symbols. Although it is powerful algorithm it not suitable for the systems that are concatenated with encoders and consequently iterative decoders. BCJR is a symbol by symbol classical demodulator that shows numerical problems in implementations. Log-MAP

and Max-Log-MAP algorithms are very similar to BCJR unless they are designed in logarithmic domain which eliminates the possible numerical problems that occur in BCJR. Here we are using the normalized MAX-Log-MAP demodulation method.

1.1.2.1 Normalized Log-MAP Algorithm

The symbol-by-symbol maximum a posteriori (MAP) decoder is discussed in this section. The MAP decoding algorithm is a recursive technique that computes the Log-Likelihood Ratio (LLR) of each bit based on the entire observed data block of length N. The starting point of deviating this algorithm is to estimate the bit or symbol using the observations from the channel[16, 15].

$$\begin{aligned} \hat{u}_i &= \arg\max P\left(u_i|y\right) = \arg\max P\left(u_i, y\right)/P\left(y\right) \\ &= \arg\max P\left(u_i, y\right) = \operatorname{argmax} \sum_{(\sigma_{i-1},\sigma_i)\in s_l} P\left(\sigma_{i-1}, \sigma_i, y\right) \end{aligned} \tag{9}$$

where $P\left(\sigma_{i-1}, \sigma_i, y\right)$ can be simplified as

$$\begin{aligned} &P\left(\sigma_{i-1}, \sigma_i, y\right) = P\left(\sigma_{i-1}, \sigma_i, y_i, y_1^{i-1}, y_{i+1}^N\right) = \\ &P\left(\sigma_{i-1}, \sigma_i, y_i, y_1^{i-1}\right) \times P\left(y_{i+1}^N|\sigma_{i-1}, \sigma_i, y_i, y_1^{i-1}\right) = \\ &P\left(\sigma_{i-1}, y_1^{i-1}\right) \times P\left(\sigma_i, y_i|\sigma_{i-1}, y_1^{i-1}\right) \times P\left(y_{i+1}^N|\sigma_i\right) = \\ &P\left(\sigma_{i-1}, y_1^{i-1}\right) \times P\left(\sigma_i, y_i|\sigma_{i-1}\right) \times P\left(y_{i+1}^N|\sigma_i\right) \end{aligned} \tag{10}$$

where σ_{i-1} and σ_i represent the previous state and current state in the trellis diagram and y_1^{i-1} and y_{i+1}^N are the following vectors.

$$\begin{aligned} y_1^{i-1} &= (y_1, \ldots, y_{i-1}) \\ y_{i+1}^N &= (y_{i+1}, \ldots, y_N) \end{aligned} \tag{11}$$

At this point we define $\alpha_{i-1}\left(\sigma_{i-1}\right)$, $\gamma\left(\sigma_i, \sigma_{i-1}\right)$ and $\beta_i\left(\sigma_i\right)$ as

$$\begin{aligned} \alpha_{i-1}\left(\sigma_{i-1}\right) &= P\left(\sigma_{i-1}, y_1^{i-1}\right) \\ \gamma\left(\sigma_i, \sigma_{i-1}\right) &= P\left(\sigma_i, y_i|\sigma_{i-1}\right) \\ \beta_i\left(\sigma_i\right) &= P\left(y_{i+1}^N|\sigma_i\right) \end{aligned} \tag{12}$$

which result in the following compact form for estimating the transmitted symbol.

$$\hat{u}_i = \text{argmax} \sum_{(\sigma_{i-1},\sigma_i)\in s_l} \alpha_{i-1}(\sigma_{i-1}) \times \gamma(\sigma_i, \sigma_{i-1}) \times \beta_i(\sigma_i) \tag{13}$$

It means that calculating the values of α, β and γ is enough to utilize this algorithm. Forward recursion and backward recursion are the methods that are used for calculating α and β values. The parameters and α and β need to be initialized and finalized respectively so that the algorithm will be working properly. Usually β is terminated at state 0 and α is initialized at any state based on the transmitted bitstream.

$$\begin{aligned} \alpha_0(\sigma_0) &= P(\sigma_0) \\ \beta_N(\sigma_N) &= P(\sigma_N) \end{aligned} \tag{14}$$

Here is the forward recursion equation for α and the backward recursion equation for β.

$$\alpha_i(\sigma_i) = \sum_{\sigma_{i-1},\sigma_i\in s_l} \alpha_{i-1}(\sigma_{i-1})\,\gamma_i(\sigma_{i-1},\sigma_i) \tag{15}$$

$$\beta_{i-1}(\sigma_{i-1}) = \sum_{\sigma_{i-1},\sigma_i\in s_l} \beta_i(\sigma_i)\,\gamma_i(\sigma_{i-1},\sigma_i) \tag{16}$$

According to 15 and 16, α and β can be calculated based on γ. γ is a parameter that depends on the priori information of the transmitted bits which can be mathematically proved in the following derivations.

$$\begin{aligned} &\gamma(\sigma_i, \sigma_{i-1}) = P(\sigma_i, y_i|\sigma_{i-1}) = P(\sigma_i|\sigma_{i-1}) \times P(y_i|\sigma_{i-1}, \sigma_i) = \\ &P(u_i) \times P(y_i|u_i) = P(u_i) \times P(y_i|c_i) \end{aligned} \tag{17}$$

Assuming the channel to be modeled as AWGN the γ values can be computed like

$$\gamma(\sigma_i, \sigma_{i-1}) = P(u_i)/(\pi N_0)^{n/2} \times \exp\left(-\|y_i - c_i\|^2/N_0\right) \tag{18}$$

The posteriori likelihood values are computed as below.

$$\begin{aligned} &L(u_i) = \ln(P(u_i = 0|y)/P(u_i = 1|y)) = \\ &\ln(P(u_i = 0, y)/P(u_i = 1, y)) = \\ &\ln\left(\frac{\sum_{(\sigma_{i-1},\sigma_i)\in s_0} \alpha_{i-1}(\sigma_{i-1})\times\gamma(\sigma_i,\sigma_{i-1})\times\beta_i(\sigma_i)}{\sum_{(\sigma_{i-1},\sigma_i)\in s_1} \alpha_{i-1}(\sigma_{i-1})\times\gamma(\sigma_i,\sigma_{i-1})\times\beta_i(\sigma_i)}\right) \end{aligned} \tag{19}$$

When no additional data is available, the information sequence is assumed equiprobable.

$$P(u_i = 0) = P(u_i = 1) = 0.5 \tag{20}$$

As described earlier, MAP algorithm is computationally very intensive for most applications and it is not suitable for chip design. In fact, the fixed-point representation of the MAP decoding variables requires between 16 to 24 bits. This motivates us to switch to Log-MAP algorithm which eliminates the numerical problems of the previous one. In which $\hat{\alpha}$, $\hat{\beta}$ and $\hat{\gamma}$ are the equivalents of α, β and γ in logarithmic domain and the likelihood ratios will be updated as.

$$L(u_i) = \ln\left(\frac{\sum_{(\sigma_{i-1},\sigma_i)\in s_0} \exp\left(\hat{\alpha}_{i-1}(\sigma_{i-1}) + \hat{\gamma}(\sigma_i,\sigma_{i-1}) + \hat{\beta}_i(\sigma_i)\right)}{\sum_{(\sigma_{i-1},\sigma_i)\in s_1} \exp\left(\hat{\alpha}_{i-1}(\sigma_{i-1}) + \hat{\gamma}(\sigma_i,\sigma_{i-1}) + \hat{\beta}_i(\sigma_i)\right)}\right) \tag{21}$$

At the end of the algorithm final decision is made based on the value of the Likelihood ratio for each symbol.

$$\hat{u}_i = \begin{cases} 0 & L(u_i) \geq 0 \\ 1 & else \end{cases} \tag{22}$$

1.2 Low Density Parity Check Codes (LDPCs)

Low Density Parity Check Codes (LDPCs) are linear block codes that are originally invented in the early 1960's by Robert Gallager [17], and have experienced an amazing comeback after popularity of iteratively decoded codes like turbo codes. In fact these codes are competitors of turbo codes and outperform these codes if designed properly. LDPCs are characterized by a sparse parity check matrix. In fact the coding gain of LDPCs comes from the randomness in generating the parity check matrix. These codes perform within 0.004 dB of Shannon capacity in case of optimal decoding. Due to excellent coding gain of these codes are adopted in several communication standards such as DVB-S2 and WiMAX (802.16e)[18, 19].

1.2.1 Low Density Parity Check Matrix

LDPCs (also called Gallager codes) are a powerful coding family which fall into the category of linear block codes. A generator matrix G specifies characteristics of this coding scheme which include the code-word structure and the overall encoding procedure.

$$x = Gu \tag{23}$$

where G is a $N \times K$ matrix with full-column rank, u is a length K column vector representing the bitstream, and x is a length N vector for the code-word. The generator matrix is in systematic form if it can be written as

$$G = \begin{bmatrix} P \\ I_{K\times K} \end{bmatrix} \tag{24}$$

where $I_{K\times K}$ is an identity matrix. This linear block code can be equivalently specified by the parity-check matrix H, where $Hx = 0$ for $x = Gu$ and H, is an $M \times N$ matrix. The parity matrix H satisfies $HG = 0$. For a systematic generator matrix H can be modeled as

$$H = \begin{bmatrix} I_{K\times K} & P \end{bmatrix} \tag{25}$$

All the matrices that satisfy $HG = 0$ with a row rank of $N - K$ can be used as the parity matrix. If H has full row-rank, then $M = N - K$; otherwise, $M > N - K$. A block code defined by a parity-check matrix H has a code rate of $(N - RowRank(H))/N$ [15].

Gaussian elimination and re-ordering of columns are used to turn the original H into a systematic form. In some cases, the randomly generated parity-check matrix H does not have full row-rank, which means some parity-check equations are redundant. In such a case, a code of rate greater than $(N - M)/N$ is defined on the linearly independent rows of H, and it is still a valid parity check matrix [20].

The parity-check matrix for an LDPC code is sparse and the positions for the ones are selected in a way that no two columns have more than one check in common. Consequently the patterns similar to the following pattern are not valid.

$$\begin{bmatrix} & \vdots & & & & \vdots & \\ \dots & 1 & 0 & \dots & 0 & 1 & \dots \\ & 0 & & & & 0 & \\ & \vdots & & & & \vdots & \\ & 0 & & & & 0 & \\ \dots & 1 & 0 & \dots & 0 & 1 & \dots \\ & \vdots & & & & \vdots & \end{bmatrix} \tag{26}$$

The LDPC codes (also called Gallager codes) require the parity check matrix to have a uniform column weight t_c as well as a uniform row weight t_r which results in fixed number of ones in the columns and rows of the matrix. The following equation maintains this property.

$$t_r \times N = t_c \times M \tag{27}$$

LDPC codes with uniform or nearly uniform column weights and row weights are now referred to as the regular LDPC codes, while codes with non-uniform column weights and row weights are referred to as the irregular LDPC codes[20]. The following shows a prototype matrix for LDPC coding.

$$H = \begin{bmatrix} 1 & 1 & 1 & 1 & 0 & 0 & 0 & 0 \\ 1 & 1 & 0 & 0 & 1 & 1 & 0 & 0 \\ 1 & 1 & 1 & 1 & 1 & 1 & 1 & 1 \end{bmatrix} \tag{28}$$

1.2.2 Factor Graph Representation

Factor graph is graphical model for calculating the marginal distributions in decoding algorithms such as sum-product algorithm. Identification of the conditional

dependency allows factorization of the joint probability to the product of conditional probabilities, which is essential in the derivation of the sum-product decoding algorithm. Factor graphs are used for factorization of joint probabilities to the product of conditional probabilities. A factor graph representation of a LDPC code contains two types of nodes, the "bit" nodes and the "check" nodes. Each bit node corresponds to a bit in the codeword, and each check node represent a parity check equation. A bit node will be connected to a check node if the bit node contributes to the equation of the corresponding check node. This connection is referred to as an edge.In the following (29) shows the equations for code word x that correspond to the prototype parity matrix in (28) and Fig.1 shows the factor graph for the prototype parity matrix in (28).

$$\begin{aligned} x_1 + x_2 + x_3 + x_4 &= 0 \\ x_1 + x_2 + x_5 + x_6 &= 0 \\ x_1 + x_2 + x_3 + x_4 + x_5 + x_6 + x_7 + x_8 &= 0 \end{aligned} \tag{29}$$

There are other graphical models with similar functionality as factor graphs such as

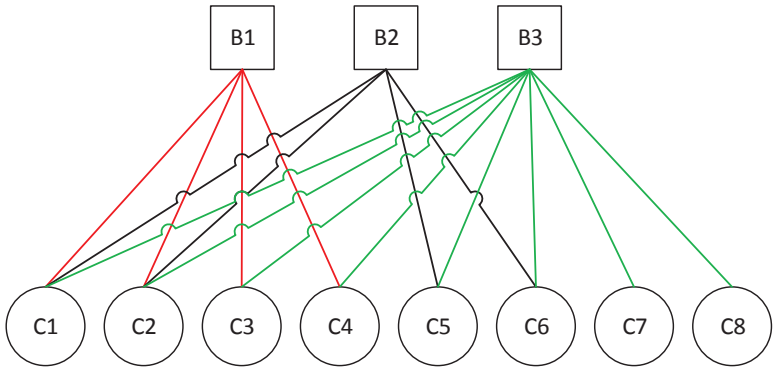

Figure 1: Factor Graph for Prototype Matrix H

Tanner graphs which can be converted to factor graphs easily. In other words, factor graphs are a straightforward generalization of these Tanner graphs [21].

1.2.3 Decoding Algorithm : The Sum-Product Algorithm

The two main algorithms used to decode LDPC codes are the bit-flipping algorithm and the sum-product algorithm. The latter is also referred to as the belief propagation algorithm. The bit-flipping algorithm is a hard decision decoding algorithm with low complexity whereas sum-product algorithm is a soft decision algorithm with higher complexity.Sum-product algorithm is a special class of a group of iterative decoding methods called belief propagation methods. The reason for this appellation is that at each round of the algorithms messages are passing back and forth between the check nodes and bit nodes which are connected across an edge in the factor graph. It is clear that the number of operations that this algorithm performs depends on the number of edges in the graph. Hence, the algorithm runs in time linear in the block length of the code.

There are two main assumptions that make the basis for belief propagation methods. The first one is called independency assumption, which reflects the fact that the message that is conveyed between each bit node and check node is independent of the previous round. The second assumption is that the information inherent in the messages is of binary nature, hence we only need to keep track of one parameter that is the probability of transmitting the messages [22].

Here is an example of factorization of the a posteriori probability in a sum-product format for a bit node in the aforementioned prototype matrix.

$$
\begin{aligned}
&p\left(x_1|y_1^8,H\right)=\sum_{x_2^5}p\left(x_1,x_2^5|y_1^8,H\right)= \\
&\sum_{x_2^5}p\left(x_1|H\right).p\left(y_1|x_1,H\right).p\left(x_2^8|y_1,x_1,H\right).p\left(y_2^8|x_1^8,y_1,H\right)= \\
&p\left(x_1|H\right)\times p\left(y_1|x_1,H\right)\times\sum_{x_2^5}p\left(x_2^4|x_1,H\right)p\left(y_2|x_2\right).p\left(y_3|x_3\right).p\left(y_4|x_4\right)\times \\
&\sum_{x_5^6}p\left(x_5^6|x_1,H\right).p\left(y_5|x_5\right).p\left(y_6|x_6\right)\times\sum_{x_7^8}p\left(x_7^8|x_1,H\right).p\left(y_7|x_7\right).p\left(y_8|x_8\right)
\end{aligned}
\tag{30}
$$

These marginal probabilities can be rewritten with the following notation.

$$p\left(x_1|y_1^8, H\right) = p\left(x_1|H\right) \times p\left(y_1|x_1, H\right) \times r_{c_1 \to x_1} \times r_{c_2 \to x_1} \times r_{c_3 \to x_1} \tag{31}$$

In which the first term shows the a priori probability and the second term corresponds to the channel information and the last three are holding the extrinsic information from the check nodes. This is an example of showing the marginal probability in sum product form. This procedure can be done in the other direction when the check nodes are trying to update their information about all the bits that are connected to them visa an edge in the factor graph. After this step is done, the extrinsic information about bits are conveyed to bits in order to update the a posteriori probability of each bit at (31). This procedure repeats until the stop criterion is satisfied.

1.2.4 The Sum-Product Algorithm Notations and Steps

In sum-product decoding of an LDPC code, $M(l)$ denotes the set of check nodes that are connected to bit node l which corresponds to "1"s in the l^{th} column of the parity-check matrix; and $L(m)$ denotes the set of bits that participate in the m^{th} parity-check equation which corresponds to the "1"s in the m^{th} row of the parity check matrix. $L(m) \setminus l$ represents the set $L(m)$ with the l^{th} bit excluded; and $M(l) \setminus m$ represents the set $M(l)$ with the m^{th} check excluded. $q_{l \to m}$ denotes the probability that bit node l sends information to check node m. $r_{m \to l}$ denotes the probability that m^{th} check node gathers infromation for the l^{th} bit. In fact this information hold the ratio of the probabilities of being 0 to 1 in decimal or logarithmic domain which are called likelihood ratios or log-likelihood ratios. The main goal of using sum-product algorithm is to find the a posteriori information about every bit. This procedure is done through gathering the extrinsic information from all the check nodes that are connected to the bits across an edge and combining this information to calculate the a posteriori probabilities. In the notations mentioned above $r_{m \to l}$ corresponds to the extrinsic information that check node m provides about the bit node l.

The iteration steps of sum-product algorithm is discussed with details in the following.

Initialization

An initial a priori information is assigned to each bit node.

$$q_{l\to m} = p\left(y_l|x_l\right) \tag{32}$$

Step 1: Checks to bits

Each check node updates its extrinsic information about the bit nodes.

$$r_{m\to l} = \sum_{x_{\hat{l}}:\hat{l}\in L(m)\backslash l} p\left(x_{\hat{l}}|x_l, H\right) \times \prod_{L(m)\backslash l} q_{l\to m} \tag{33}$$

Step 2: Bits to checks

Each bit node uses the information it gets from the check nodes to update its a posteriori probability.

$$q_{l\to m} = \eta_{ml} p_l \prod_{\hat{m}\in M(l)\backslash m} r_{\hat{m}\to l} \tag{34}$$

where η_{ml} is the normalization factor.

Step 3: Check stop criterion

The decoder will go back to step 1 and repeat the whole process and continues the iterations till the condition $Hx = 0$ is satisfied. The next step is to make the final decision about the transmitted bits according to each bit's a posteriori probability using hard decision methods.

1.2.4.1 Decoding In Log Domain

In order to avoid numerical problems in implementation the same algorithm is designed in logarithmic domain. Here are the steps of sum-product algorithm in logarithmic domain.

Initialization

An initial a priori information is assigned to each bit node.

$$\begin{aligned} L\left(q_{l\to m}\right) &= {}^{2}\!/_{\sigma^2} y_l \\ L\left(r_{m\to l}\right) &= 0 \end{aligned} \tag{35}$$

Step 1: Checks to bits

Each check node updates its extrinsic information about the bit nodes.

$$L\left(r_{m\to l}\right) = 2\tanh^{-1}\left(\prod_{\hat{l}\in L(m)\setminus l}\tanh\left(L\left(q_{l\to m}\right)/2\right)\right) \tag{36}$$

Step 2: Bits to checks

Each bit node uses the information it gets from the check nodes to update its a posteriori probability.

$$L\left(q_{l\to m}\right) = L\left(p_l\right) + \sum_{\hat{m}\in M(l)\setminus m} L\left(r_{m\to l}\right) \tag{37}$$

Step 3: Check stop criterion

The decoder will go back to step 1 and repeat the whole process and continues the iterations until the stop criteria is satisfied. The total a posteriori probability for every bit is calculated by summing the information from all the check nodes that connect to that specific bit.

$$L\left(q_l\right) = L\left(p_l\right) + \sum_{\hat{m}\in M(l)} L\left(r_{m\to l}\right) \tag{38}$$

1.2.5 Sum-Product Algorithm, Pros and Cons

Sum-product is a very feasible algorithm for practical purposes.This algorithm for decoding the LDPC codes can be implemented in parallel. At each iteration, all the nodes operate simultaneously, based on the input belief from the previous iteration, and "broadcast" the updated belief to their connected neighbors for the next iteration decoding. This leads to less decoding delay and high-throughput designs. However, LDPC codes may require more iterations for the decoding process to converge in comparison with other powerful coding schemes.The decoding complexity of LDPC codes is proportional to the column weights of the parity-check matrix, and is usually lower than that of a turbo code. Sum-product algorithm works well on factor graphs that do not contain short cycles. For a bipartite graph, the shortest possible cycle

length is four. Efficient LDPC codes avoid length-four cycles in the factor graph representation [15, 20, 23].

1.2.6 LDPC Codes For WiMAX (802.16e)

The LDPC code is based on a set of one or more fundamental LDPC codes. Each of the fundamental codes is a systematic linear block code. The code rate and block length of the code are the main factors that effect the coding gain, assuming a fixed decoding algorithm. WiMAX physical layer standard deals with the open problem of choosing the proper parity check matrix and proposes 114 matrices with different coding rates and block lengths. All these codes provide an acceptable coding gain which makes them feasible for implementation purposes. For code rates 1/2, 3/4 A and B code, 2/3 B code and 5/6 codes are available in this standard [18].

Each LDPC code in the set of LDPC codes is defined by a matrix H of size M-by-N, where N is the length of the code and M is the number of parity check bits in the code. The number of systematic bits is $k = N - M$.

The matrix H is defined as:

$$H = \begin{bmatrix} P_{0,0} & P_{0,1} & P_{0,2} & \cdots & P_{0,n_b-2} & P_{0,n_b-1} \\ P_{1,0} & P_{1,1} & P_{1,2} & \cdots & P_{1,n_b-2} & P_{1,n_b-1} \\ P_{2,0} & P_{2,1} & P_{2,2} & \cdots & P_{2,n_b-2} & P_{2,n_b-1} \\ \vdots & \vdots & \vdots & & \vdots & \vdots \\ P_{m_b-1,0} & P_{m_b-1,1} & P_{m_b-1,2} & \cdots & P_{m_b-2,n_b-2} & P_{m_b-1,n_b-1} \end{bmatrix} = P^{H_b} \qquad (39)$$

where $P_{i,j}$ is one of a set of z-by-z permutation matrices or a z-by-z zero matrix. The matrix H is expanded from a binary base matrixH_b of size m_b-by-n_b, where $M = z \times m_b$and $N = z \times n_b$,with z an integer larger than 1. The base matrix is expanded by replacing each 1 in the base matrix with a z-by-z permutation matrix, and each 0 with a z-by-z zero matrix. The base matrix size z is an integer equal to 24 in WiMAX [18].

The permutations used are circular right shifts, and the set of permutation matrices contains the z-by-z identity matrix and circular right shifted versions of the identity matrix. Because each permutation matrix is specified by a single circular right shift, the binary base matrix information and permutation replacement information can be combined into a single compact model matrix H_{mb}. The model matrix H_{mb} can then be directly expanded to H. Each 1 in H_{mb} is assigned a shift size of 0, and is replaced by a z-by-z identity matrix when expanding to H. Codes with rates 1/2, 3/4 A and B , 2/3 B and 5/6 are the available in this standard.

Long block length increases the coding gain as well as the latency of the decoder. This leads us to choose the parity check matrices with block length of 576 and test its performance over memoryless AWGN channel with bpsk modulation. Results of BER for WiMAX codes are illustrated in the following figure.

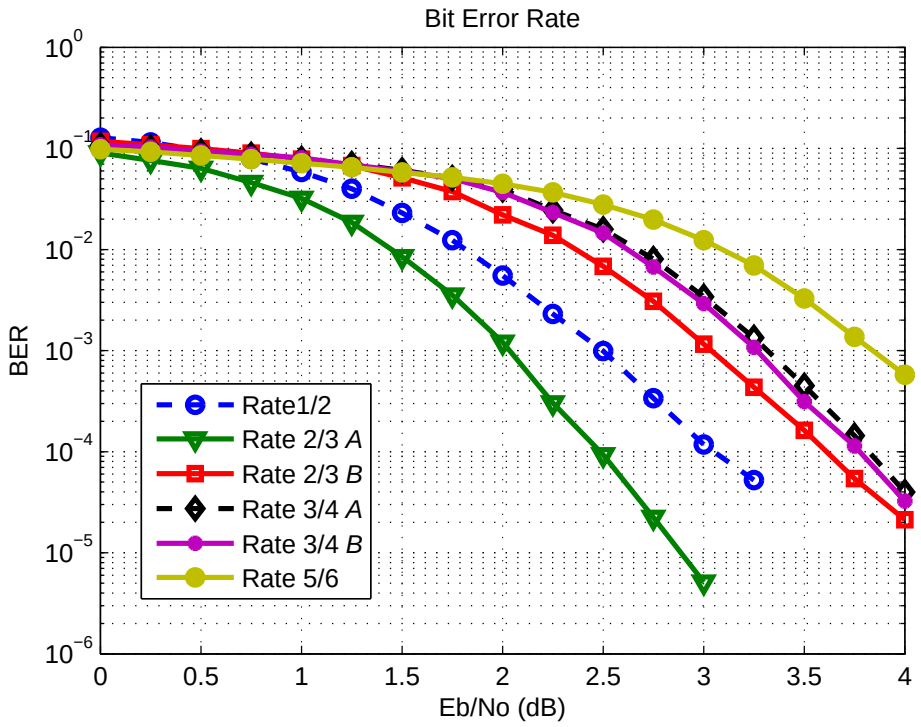

Figure 2: BER of LDPC-coded bpsk for AWGN channel for WiMAX codes.

1.3 Jamming Signals

There are several jamming strategies that a jammer can use against an anti-jamming (AJ) target. These strategies, which are illustrated on Fig.3, are separated to two main groups of noise jamming signals and tone jamming signals. Within the first category are wideband noise, partial-band noise and narrowband noise signals. In the first two jamming signals occupy a portion of or the entire spectrum in use by the AJ system, but the signals stay in one place in the spectrum. In the second category are tone jammers that can be applied to both direct sequence spread spectrum (DSSS) and frequency hopping spread spectrum (FHSS) AJ signals. A single tone can be used against DSSS or FHSS when the latter is attempted with the follower strategy. Usually the placement of these tones on the spectrum is based on some further knowledge of the target which is to be jammed [24, 25].

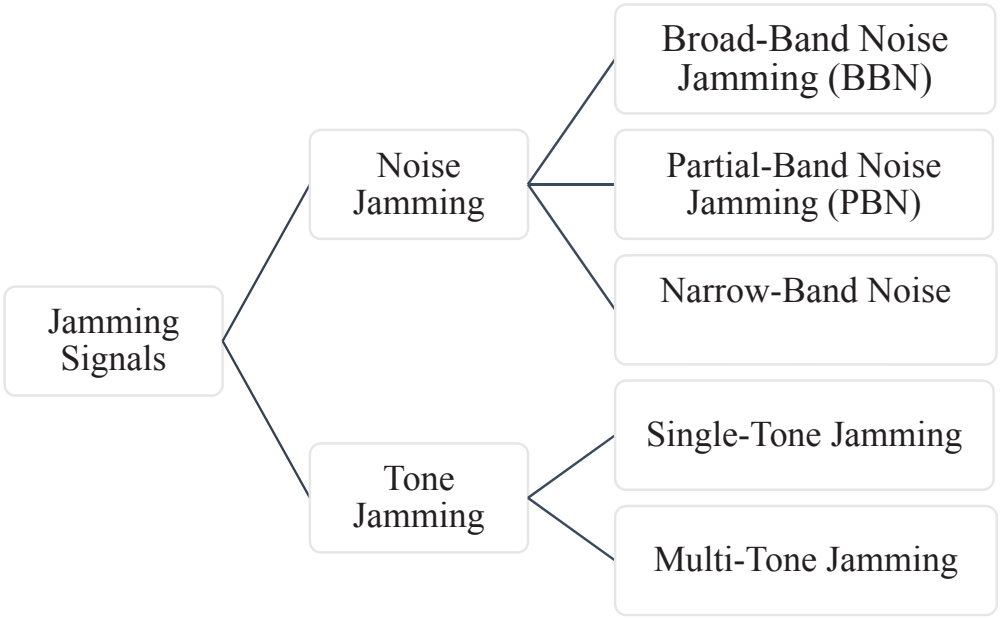

Figure 3: Jamming strategies.

CHAPTER II

OPTIMAL CHOISE OF PARAMETERS FOR LDPC-CODED CPM

In this chapter, we address the problem of selecting the optimal transmission parameters in an LDPC-coded CPM system to satisfy a given spectral efficiency subject to a constraint on the demodulator complexity. We describe the system model, waveform structure, the search procedure and the proper LDPC-coded CPM scheme to satisfy the targeted requirements. Modulation index, alphabet size, pulse shape duration and code rate are the transmission parameters. We present a Monte Carlo simulation study to demonstrate the performance of the selected LDPC-coded CPM scheme with and without jamming. We also demonstrate the error rate performance of the selected scheme through Monte Carlo simulations. Then, we estimate the power spectral density and compare it with that of the conventional frequency shift keying (FSK).

2.1 LDPC-coded CPM

In an LDPC-coded CPM system, there are several transmission parameters to choose including modulation index, alphabet size, pulse shape duration and code rate which directly impact the performance. Fig. 4 illustrates the system model under consideration. The input bits are coded by LDPC encoder before being sent to the CPM modulator. Unlike the conventional FSK modulation schemes in which signals are defined over a symbol interval, CPM is defined over the entire time axis which implies inherent memory embedded with this modulation. Assuming transmission over

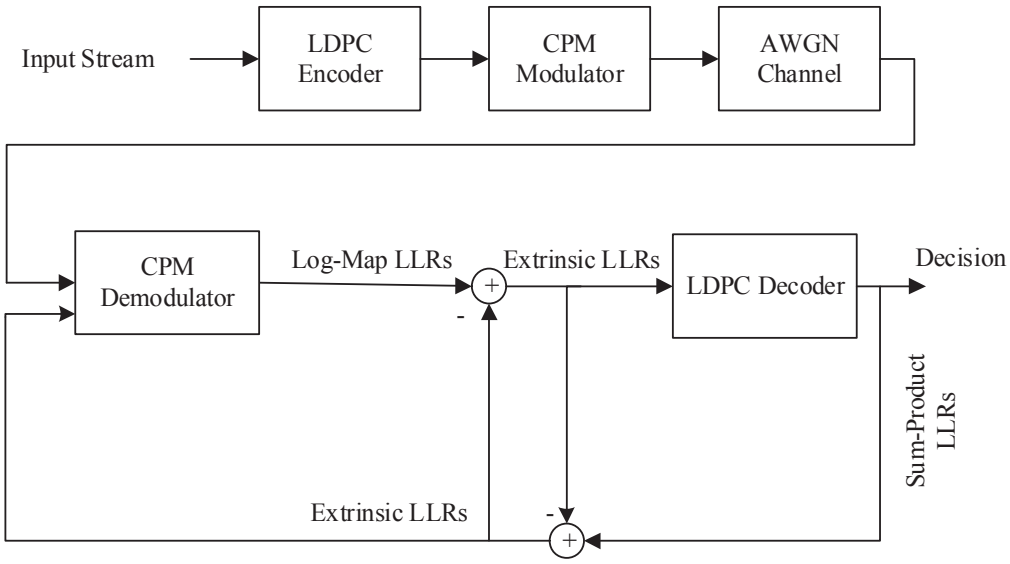

Figure 4: System model for LDPC-coded CPM.

additive white Gaussian noise (AWGN), the received signal is given by

$$r(t) = s(t) + n(t), \qquad 0 < t < NT \tag{40}$$

where N is the number of transmitted symbols, T is the symbol duration, and *n(t)* is the AWGN term which is modeled as a complex Gaussian random variable with zero mean and power spectral density of $N_0/2$. In (40), *s(t)* denotes the CPM signal and is given in details by 1-7 in chapter 1. At the receiver part, the signal is first demodulated using normalized MAX-Log-MAP algorithm [26]. Low complexity and execution in probability domain makes this algorithm suitable for iterative receivers [26]. After demodulation, the bits are passed through channel decoder. We employ sum-product algorithm [23] which is a belief propagation algorithm and is based on calculating the marginal distributions of the nodes on factor graphs. This algorithm is selected because of its high code gain and easy combination with MAP demodulator [8]. In the concatenated iterative decoder, these probabilities are used as the extrinsic information. Each of these algorithms produces soft output data that holds extrinsic information about the transmitted bits. At both decoder and demodulator, this information is extracted and passed on to the next one for another round of the

iteration.

2.2 Exhaustive Search

Our objective is to select the best CPM parameters and outer LDPC code to satisfy a given spectral efficiency subject to a constraint on the demodulator complexity. The CPM parameters which directly affect spectral efficiency are h, M and L. For modulation index, we define the set $\mathbf{H} = \{0.1, 0.2, 0.3, 0.4, 0.5, 0.6, 0.7, 0.8, 0.9\}$ which includes rational values less than one with 0.1 increments. As seen in (2), h is a multiplication factor in the phase of the waveform and its values less than unity will ensure spectrum compactness of the CPM signal. We choose the set $\mathbf{M} = \{2, 4, 8\}$ as the set of available alphabet sizes. We limit the alphabet size by $M = 8$ because increasing M results in a waveform that no longer meets the out of band emission requirements [9]. For the pulse shaping symbol length, we define the set $\mathbf{L} = \{1, 2, 3, 4, 5\}$ where $L = 1$ indicates that there is no intersymbol interference and indicates that the symbols interfere with each other. The former is called "full response CPM" and the latter is called "partial response CPM" [15]. $L = 1$ refers to an ideal case which is not practically feasible, however it is less complex to deal with this case due to elimination of intersymbol interference. $L > 1$ is more complex from implementation point of view however it is a more realistic one.

Our candidate pool includes any permutation of these CPM parameters which contains 135 different cases whose values are drawn from **H**, **M** and **L**. In our system, we employ LDPC encoders with dual diagonal parity check matrices with rates 0.5 and 0.75, and block lengths of 576. These matrices are chosen from the WiMAX standard [18]. Therefore, there is a total number of 270 candidates in our pool.

Our search procedure depends on three performance metrics, namely bit error rate (BER), spectral efficiency and demodulator complexity. The demodulator complexity

is defined as the number of the states in the trellis diagram which refers to the state machine representation of the CPM. Assuming h is a rational number which can be represented by p/q where p and q are relatively prime integers, the number of states is given by $N_{states} = 2qM^{L-1}$ if p is an odd number. Otherwise, it is given by $N_{states} = qM^{L-1}$. We first perform an elimination based on the complexity and exclude the candidate schemes with $N_{states} > 160$. This reduces the number of schemes in the candidate pool to 204. The spectral efficiency is defined as

$$\eta = \frac{\log_2(M)R}{W} \tag{41}$$

where R is the code rate and W is the 20 dB bandwidth (i.e. the bandwidth where the power spectral density lies within 20 dB of the of its peak)[27]. For each of the LDPC-coded CPM candidate schemes, we evaluate the power spectral density (PSD) using Welch's method [28], calculate the 20 dB bandwidth and calculate the spectral efficiency based on (41).

The spectral efficiency of the CPM system depends on the parameters of CPM among which modulation index and symbol length of pulse shape play the most important roles. The following figures expolre the effect of aforementioned parameters on the PSD of the signal.

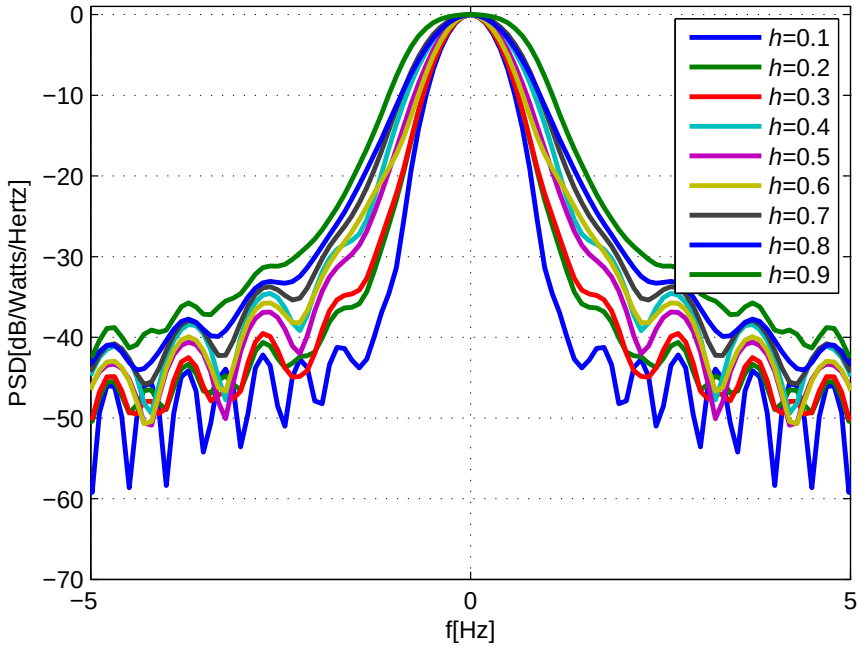

Figure 5: Effect of modulation index h on PSD of CPM signal.

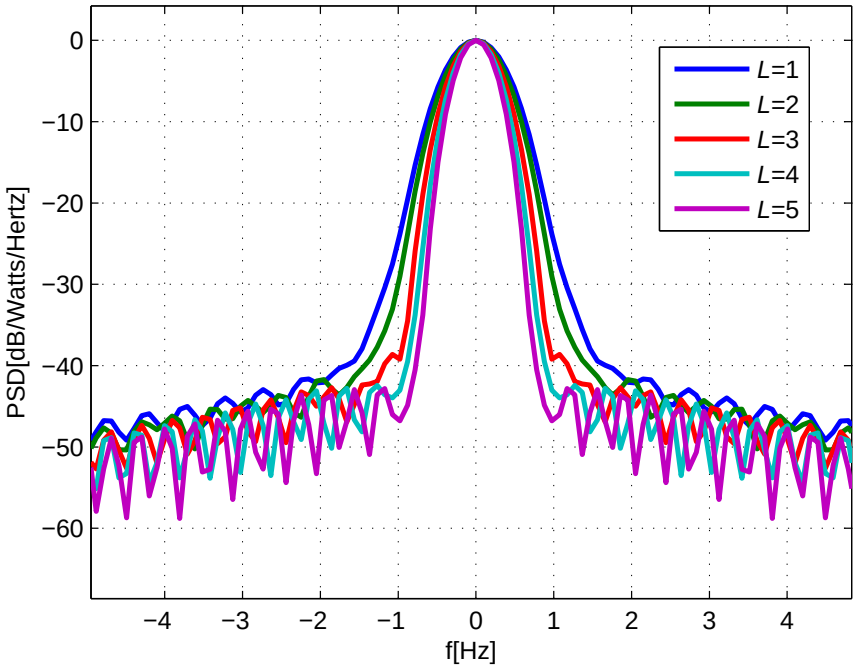

Figure 6: Effect of pulse shape duration L on PSD of CPM signal.

Fig.5 illustrates the effect of modulation index on PSD and consequently its effect on the spectral efficiency of the system. Alphabet size M is assumed to be 2 and symbol length of pulse shape L is unity in the simulations. This figure shows that increasing the value of h leads to wider PSD curves which reflects the fact that modulation index is inversely proportional to spectral efficiency of the system. Spectral efficiency is calculated through (41). For example for $h = 0.9$ the spectral efficiency is 0.4013 whereas for lower modulation indexes like $h = 0.2$ and $h = 0.1$ spectral efficiency equals to 0.6178 and 0.7014 respectively [27, 29, 30].

Fig.6 explores the effect of symbol length of pulse shape on the PSD of the signal. Modulation index, h is assumed to be 0.2 and alphabet size, M is assumed to be 2 here. The figure demonstrates that increasing this parameter results in more compact PSD curves. It means that increasing the length of pulse shape increases the spectral efficiency of the signal. For instance, for $L = 1$, $L = 2$ and $L = 4$ the spectral efficiency from (41) equals to 0.6178, 0.7245 and 0.9109 respectively. It can be inferred from the values of spectral efficiency that the spectral efficiency of $L = 4$ is 1.45 times that of $L = 1$ assuming fixed parameters for h and M [27, 29, 30].

In the second elimination step, all candidates with $\eta_{CPM} < 0.60$ are excluded from the search pool. This leaves us with 35 candidate schemes which are provided in Table 1.

For the last step of search procedure, we evaluate the BER performance of each scheme in Table 1 over AWGN channel through simulations and quantify the required signal-to-noise ratio (SNR) to achieve a BER of 10^{-3}. In the simulations, we assume that the maximum number of iterations in sum-product algorithm is 10 and the total number of iterations in the iterative decoder is 3. To have a better understanding of the trade-off between power efficiency and spectral efficiency, we illustrate the trade-off performance of 35 remaining candidates in Fig. 7. To search for the best schemes in this figure, we restrict our attention to the region of performance plot where the

Table 1: Complexity, spectral efficiency and power efficiency of candidate schemes.

	M	h	L	R	N_{states}	η	SNR[dB]
C1	2	0.2	3	0.5	40	0.6158	6.00
C2	2	0.1	3	0.5	80	0.6352	4.45
C3	2	0.5	4	0.5	32	0.6064	9.40
C4	2	0.4	4	0.5	40	0.6064	6.60
C5	2	0.3	4	0.5	160	0.6284	5.43
C6	2	0.2	4	0.5	80	0.6832	6.83
C7	2	0.1	4	0.5	160	0.7008	3.10
C8	2	0.2	3	0.75	40	0.6158	4.30
C9	2	0.5	4	0.75	32	0.6064	7.81
C10	2	0.4	4	0.75	40	0.6064	4.30
C11	2	0.3	4	0.75	160	0.6284	3.50
C12	2	0.2	4	0.75	80	0.6832	4.08
C13	2	0.1	4	0.75	160	0.7008	2.71
C14	4	0.6	2	0.75	40	0.6499	14.12
C15	4	0.4	2	0.75	20	0.7680	14.01
C16	4	0.3	2	0.75	80	0.8939	12.00
C17	4	0.2	2	0.75	40	0.9249	9.76
C18	4	0.1	2	0.75	80	1.0407	7.61
C19	4	0.8	3	0.75	80	0.6983	9.58
C20	4	0.6	3	0.75	40	0.8185	13.28
C21	4	0.5	3	0.75	64	0.8440	6.80
C22	4	0.4	3	0.75	40	0.9428	13.32
C23	4	0.2	3	0.75	40	1.0723	10.36
C24	4	0.2	2	0.5	40	0.6166	12.30
C25	4	0.1	2	0.5	80	0.6938	9.46
C26	4	0.4	3	0.5	80	0.6285	16.00
C27	4	0.2	3	0.5	160	0.7149	11.48
C28	8	0.4	2	0.5	40	0.9531	19.08
C29	8	0.3	2	0.5	160	1.0812	17.20
C30	8	0.2	2	0.5	80	1.1642	18.70
C31	8	0.1	2	0.5	160	1.1811	16.00
C32	8	0.4	2	0.75	40	1.4297	18.36
C33	8	0.3	2	0.75	160	1.6217	16.57
C34	8	0.2	2	0.75	80	1.7464	18.03
C35	8	0.1	2	0.75	160	1.7717	15.11

power efficiency and spectral efficiency are both sufficiently high.

From Fig. 7, we observe that schemes **C17** (with 40 states), **C18** (with 80 states), **C21** (with 64 states), **C13** (with 160 states) and **C7** (with 160 states) are the top

candidates. Among these schemes, **C18** provides jointly high power and spectral efficiency. The required SNR value 10^{-3} for this scheme is 7.61 dB. It also achieves the best spectral efficiency, 1.0407, compared to its competitors.

The required SNRs to achieve BER = 10^{-3} for the competing schemes (i.e., **C7**, **C13**, **C17** and **C21**) are 3.10 dB, 2.71 dB, 9.76 dB and 6.80 dB respectively. Although **C7** and **C13** achieve high power efficiency, their spectral efficiency is limited to 0.7008. Therefore, **C18** becomes our choice.

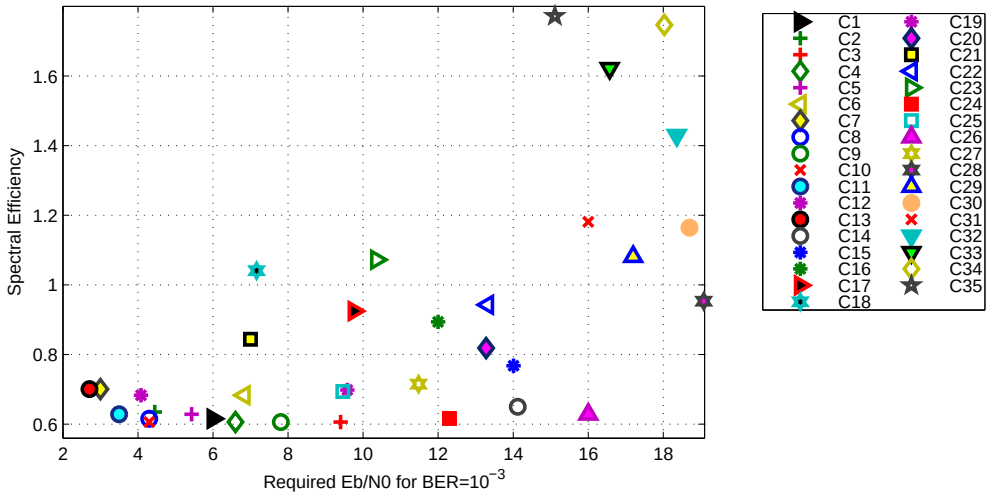

Figure 7: SNR versus spectral efficiency for candidate LDPC-coded CPM schemes.

2.3 Performance of the Selected Scheme

In this section, we present the BER performance and spectral characteristics of the selected scheme **C18**. The parameters of this scheme are $L = 2$, $h = 0.1$, $M = 4$ and uses the LDPC code with rate 0.75 and block length of 576. In Fig. 8, we present the BER performance of this scheme over AWGN. As benchmarks, we also include the performance of **C7**, **C13**, **C17** and **C21** which are strong competitors of the selected scheme as discussed above. It is obvious from Fig. 8 that **C7**, **C13** and **C21** outperform **C18**. Specifically, to achieve a BER = 10^{-3}, the required SNRs are 3.10,

2.71 and 6.80 respectively, lower than than that of **C18**. However, with its superior spectral efficiency, **C18** became our choice.

In Fig. 9, we present the BER performance of the schemes with frequency hopping over AWGN in the presence of single tone jamming. We assume that the jammer tone is selected within the channel bandwidth. We also assume an amplitude level of -3 dB for the jammer and the number of hopping channels is set to 64. Fig. 9 illustrates that **C21** has very poor performance in presence of single tone jamming. **C17** is also vulnerable to jamming compared to the other schemes. **C18**, **C13** and **C7** require 8.15 dB, 3.38 dB and 4.18 dB respectively. This shows that **C18**, **C13** and **C7** show reliable performance in presence of jamming. As discussed earlier, **C18** is superior due to its spectral compact waveform. On the other hand, low complexity of this scheme in comparison with **C13** and **C7** is the second factor that leads to selection of **C18** as the best LDPC-coded CPM scheme out of 270 candidates.

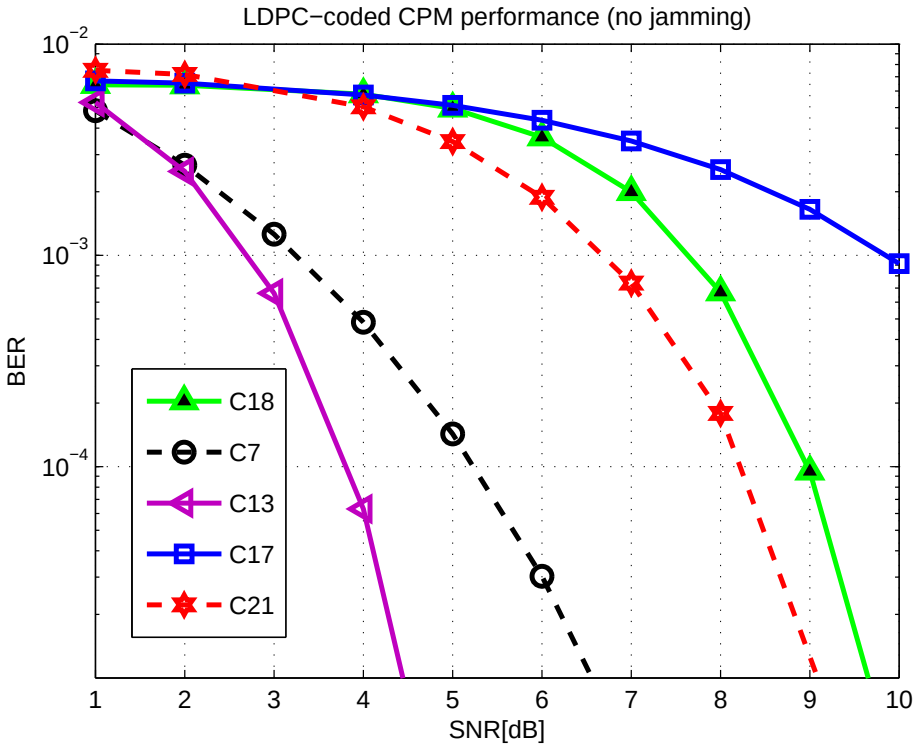

Figure 8: BER of selected scheme **C18** over AWGN channel and comparison with **C7**, **C13**, **C17** and **C21**.

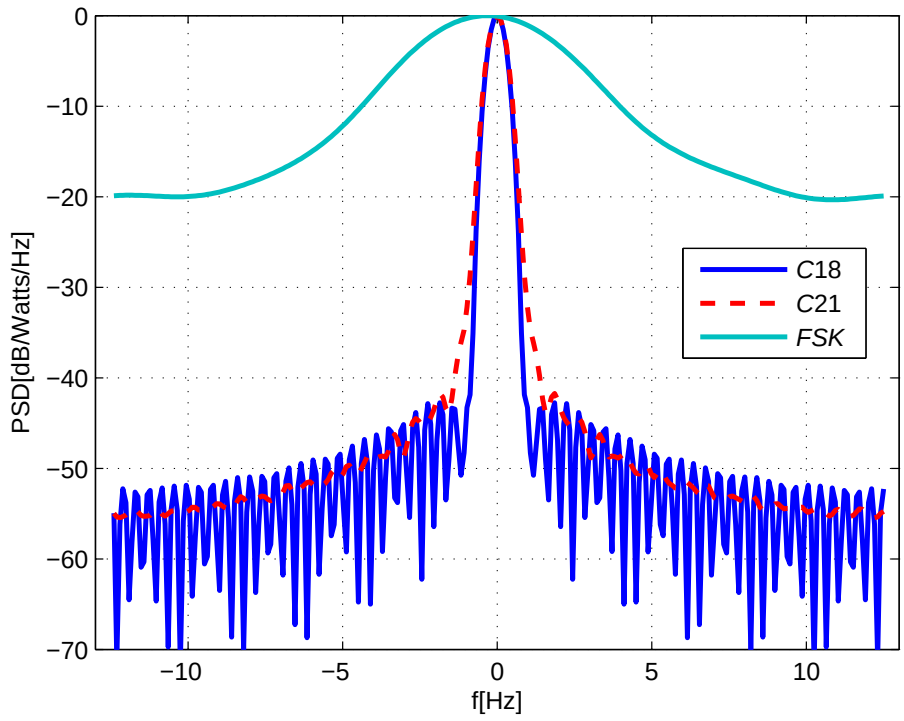

Figure 10: PSD of selected scheme **C18** and comparison with **C21** and FSK modulation.

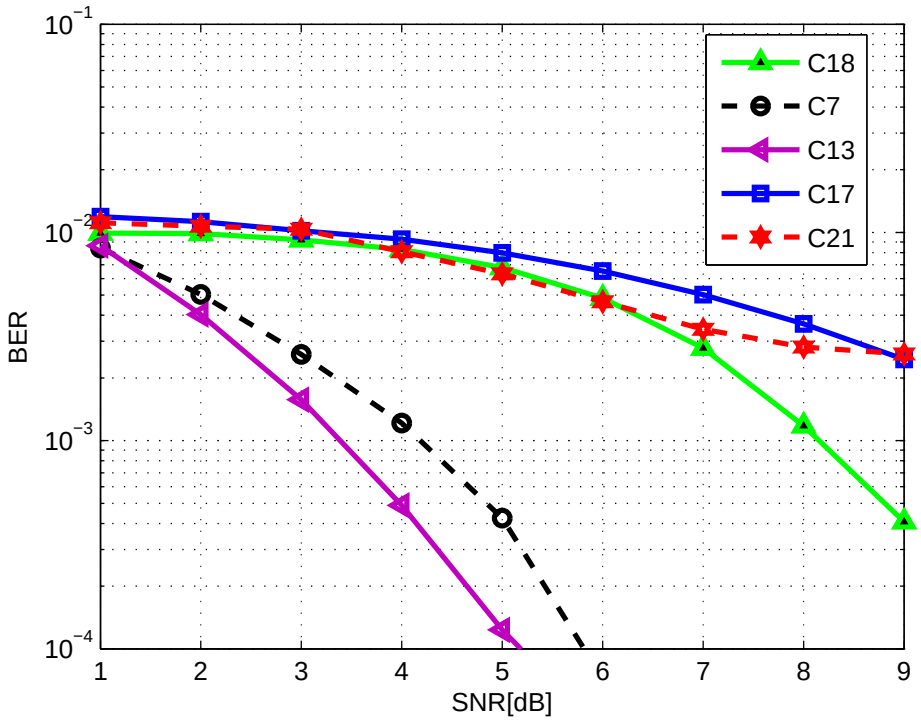

Figure 9: BER of selected scheme **C18** with frequency hopping under single tone jamming environment and comparison with **C7**, **C13**, **C17** and **C21**.

In Fig. 10, we illustrate the power spectral density of the selected scheme and compare it with that of FSK modulation and another candidate scheme (**C21**) that has good power efficiency but low spectral efficiency. It is observed that **C18** has much lower side lobes, which confirms the spectrally efficient feature of the selected CPM scheme.

2.4 Conclusion

In this chapter, we considered an LDPC-encoded CPM system and investigated the proper choice of transmission parameters such as modulation index, alphabet size, pulse shape duration and code rate. Utilizing a systematic search procedure, we identified the proper transmission parameters to achieve a targeted spectral efficiency and error rate under a constraint on demodulator complexity. We demonstrated the superior performance of selected LDPC-CPM scheme over its competitors.

CHAPTER III

LDPC-CODED CPM SYSTEM IN DIFFERENT JAMMING ENVIRONMENTS

This chapter serves the purpose of applying different jamming techniques and exploring their effects on the system using Signal to Jamming Ratio (SJR) values as evaluation metrics. The detailed explanation of classification of jamming signals is provided in chapter 1. Fig.11 illustrates the common jamming strategies that are usually employed by the adversity to kill the communication. The first four jammers fall into the category of noise jammers and the last two are tone jammers. Depending on the characteristics of the system, one of these strategies can be more powerful than the other ones. The effectiveness of these jammers mostly depends on the sort of preventive measures that are taken by the local system against them. Here the system is assumed to be equipped with frequency hopping technique as a basic mean of protection against jammers.

In this chapter, first the system is assumed to be uncoded FSK modulated transceiver. Later the transceiver is switched to the selected LDPC-coded CPM scheme which is chosen from previous chapter and the same procedure as that of uncoded FSK is repeated for the latter as well. At the end we select the strongest jammer and discuss the effect of power of jammer and number of frequency hopping channels as the basic parameters of a jammer on the overall system performance.

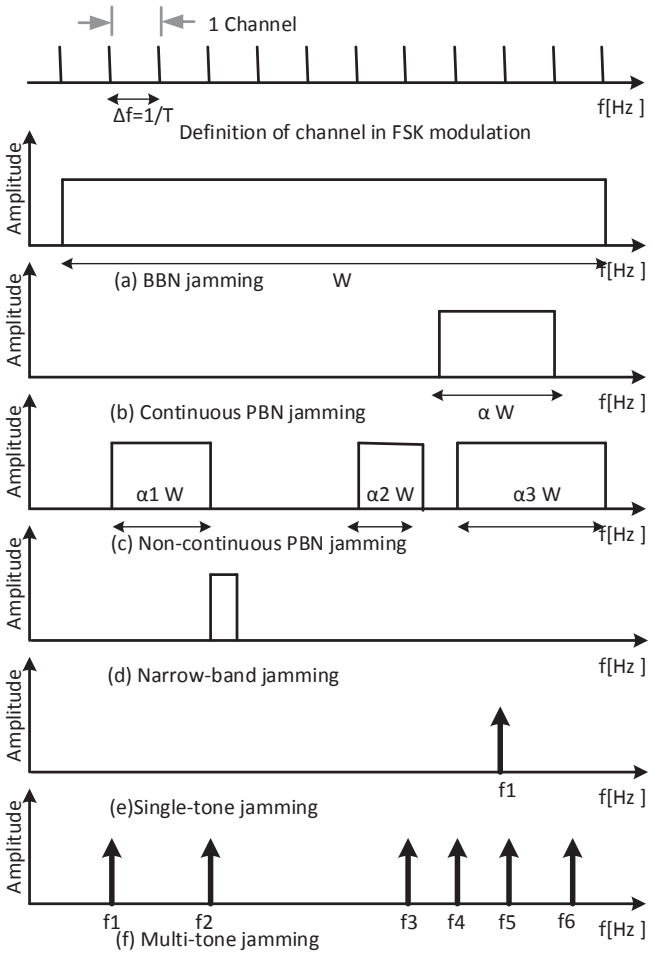

Figure 11: Representation of jamming strategies in frequency domain.

3.1 Frequency Hopping Spread Spectrum

Frequency hopping is the periodic change in the frequency of a carrier signal which is a method that has been used for many years in order to improve the security of communication systems specially in military services. This time-varying characteristic potentially endows a communication system with great strength against interference. The basic mechanism of interference suppression in a frequency-hopping system is "avoidance". When the avoidance fails, it is only temporary because of the periodic change of the carrier frequency. The impact of the interference is further mitigated by the use of channel codes, which are more essential for frequency-hopping than

for any other spread spectrum technique. There is a sequence of carrier frequencies transmitted by a frequency-hopping system which is called the frequency-hopping pattern. Hopping occurs over a frequency band called the hopping band that includes N_h frequency channels. Each frequency channel is defined as a spectral region that includes a single carrier frequency which is called the center frequency and has a bandwidth B large enough to include most of the power of a signal pulse. In any system that is equipped with frequency hopping technique there is a condition that needs to be satisfied. That is the hopping band has bandwidth $W \geq N_h B$.

Frequency hopping methods are divided in two groups of fast frequency hopping and slow frequency hopping. Fast frequency hopping occurs if there is more than one hop for each information symbol. Slow frequency hopping occurs if one or more information symbols are transmitted in the time interval between frequency hops. Fast frequency hopping is an option only if a hop rate that exceeds the information-symbol rate can be implemented. Slow frequency hopping is preferable because the transmitted waveform is much more spectrally compact and the overhead cost of the switching time is reduced [31]. Therefore, we are using slow frequency hopping in the simulations of this chapter.

3.2 Effect of Jamming Signals on FSK modulated systems

3.2.1 Broadband noise (BBN) jamming and Partial-band Noise (PBN) jamming

Broadband noise (BBN) jamming places noise energy across the entire width of the frequency spectrum used by the target communication systems. It is also called full band jamming and is sometimes called barrage jamming [24]. The latter term, however, also refers to cases where less than the full band is jammed. This type of jamming is useful against all forms of AJ communications. It is generally useful for coverage of an area for screening purposes as well. In system implementation timing and synchronization play important roles. That's why BBN jamming raises the

background noise level and tries to attack the synchronization and tracking processes of the adversary.

BBN jamming is represented in Fig.11(a). PBN jamming is represented in Fig.11(b). The primary limitation of BBN jamming is that it results in low jamming power as this signal is spread very wide in frequency domain. It is not as effective as partial-band jamming. For the PBN jamming there is a parameter α that defines the percentage of bandwidth that is covered by the jammer. This parameter is illustrated in Fig.11(b). As discussed earlier, PBN jamming places noise-jamming energy across multiple, but not all, channels in the spectrum used by the targets.

Fig.12 demonstrates the effect of PBN jamming on the BER performance of FSK modulated system assuming various α values. BBN jamming (which means PBN with $\alpha = 1$) curve is plotted along with PBN jamming curves in which the former is basically plotted as a bench mark. The BER performance is plotted with respect to signal-to-jamming ratio (SJR) which is defined as SJR = Signal power/Jamming power, while signal to noise ratio is assumed fixed. Here, we assume that SNR = 8 dB. (In the simulations we assume that the signal is normalized and power of jammer and noise changes in the system). It is observed that as α increases and approaches to unity, the jamming effect gets weaker and and asymptotically performs the same as BBN jammers because the jamming energy spreads over a wider spectrum. Assuming SNR = 8 dB, BER is 0.006 for no jamming case which is depicted in the figure with a straight solid line as a bench mark. It is also illustrated that for achieving BER = 10^{-2} for $\alpha = 1$, $\alpha = 0.8$, $\alpha = 0.5$, $\alpha = 0.3$ and $\alpha = 0.1$ the required SJRs are -16.1 dB, -15.08 dB, -13.27 dB, -10.87 dB and -6.08 dB respectively.

Fig.13 demonstrates the effect of non-continuous PBN jamming signal on the BER performance of FSK modulation assuming various sets of α values. Specifically, we

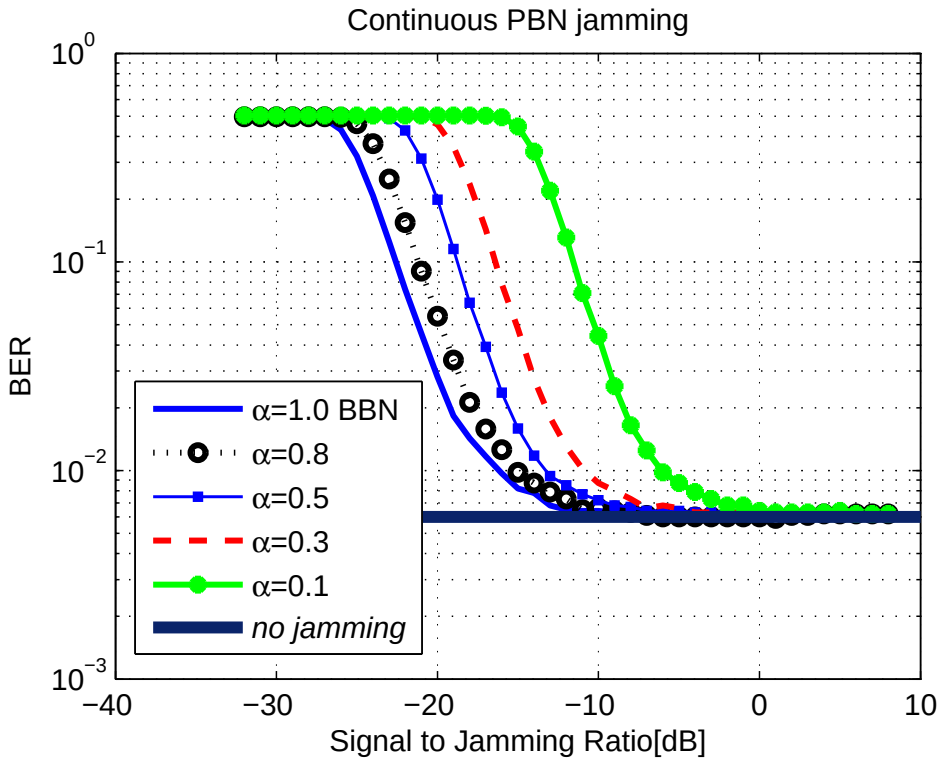

Figure 12: BER of FSK for BBN and continuous PBN with different α values for (SNR = 8 dB)

assume

$$\boldsymbol{\alpha}_1 = [0.10 \;\; 0.24 \;\; 0.30]$$

$$\boldsymbol{\alpha}_2 = [0.46 \;\; 0.24 \;\; 0.30] \tag{42}$$

$$\boldsymbol{\alpha}_3 = [0.3 \;\; 0.1 \;\; 0.1 \;\; 0.1 \;\; 0.1 \;\; 0.1 \;\; 0.1 \;\; 0.1]$$

Assuming SNR = 8 dB, BER is 0.006 for no jamming case which is depicted in Fig.13 with a straight solid line as a bench mark. It is also illustrated that for achieving BER = 10^{-3} for $\boldsymbol{\alpha}_1$,$\boldsymbol{\alpha}_2$ and $\boldsymbol{\alpha}_3$ the required SJRs are -6.18 dB, -14.70 dB and +2.90 dB respectively. It means that $\boldsymbol{\alpha}_1$ outperforms $\boldsymbol{\alpha}_2$ in terms of jamming effectiveness. In other words, BER of the system gets worse when exposed to $\boldsymbol{\alpha}_1$. Both $\boldsymbol{\alpha}_1$ and $\boldsymbol{\alpha}_2$ consist of three partial-band waveforms, but $\boldsymbol{\alpha}_2$ has a wider coverage in the spectrum. This results in a weaker jamming signal. $\boldsymbol{\alpha}_3$ shows the strongest jamming performance and the reason behind this is that it covers almost the whole spectrum using narrowband signals.

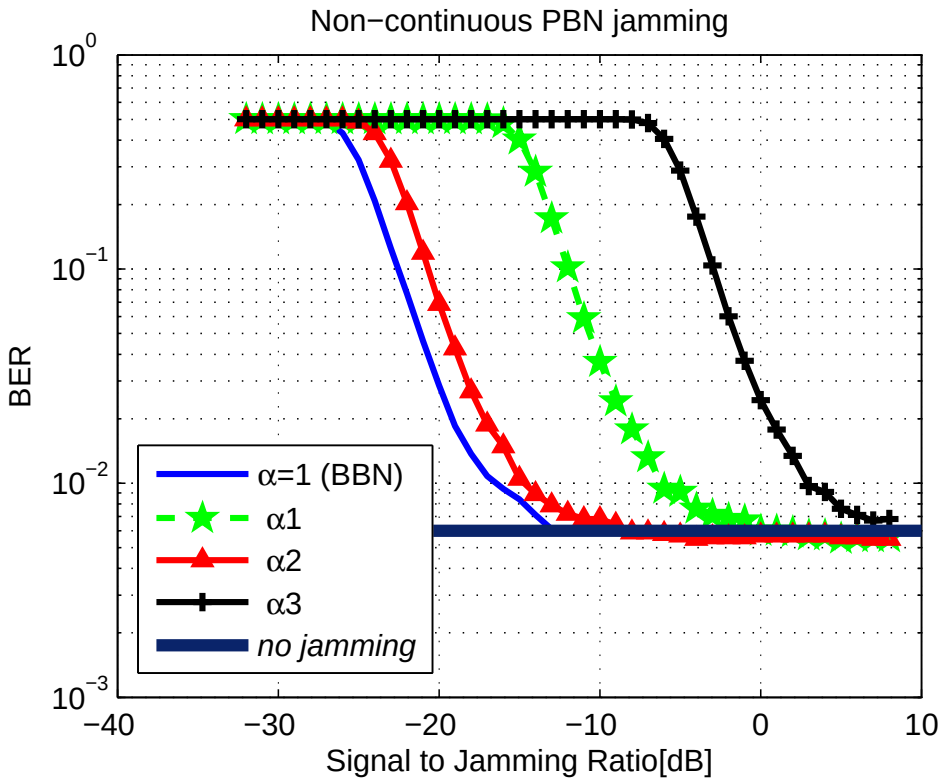

Figure 13: BER of FSK for non-continuous PBN with different sets of α values (SNR = 8 dB).

3.2.2 Narrowband noise (NBN) jamming

Narrowband noise (NBN) jamming places all of the jamming energy into a single channel. The bandwidth of this energy injection could be the whole width of the channel or it could be only the data signal width. Narrowband noise jamming is illustrated in Fig.11 (d) and its performance evaluation is illustrated in Fig.14. The narrower the channels is the stronger the jammer performs. So by dividing the available spectrum to more channels, stronger NBN jammers can be designed. Assuming SNR = 8 dB, BER is 0.006 for the no jamming case which is depicted in the figure with a straight solid line as a bench mark.

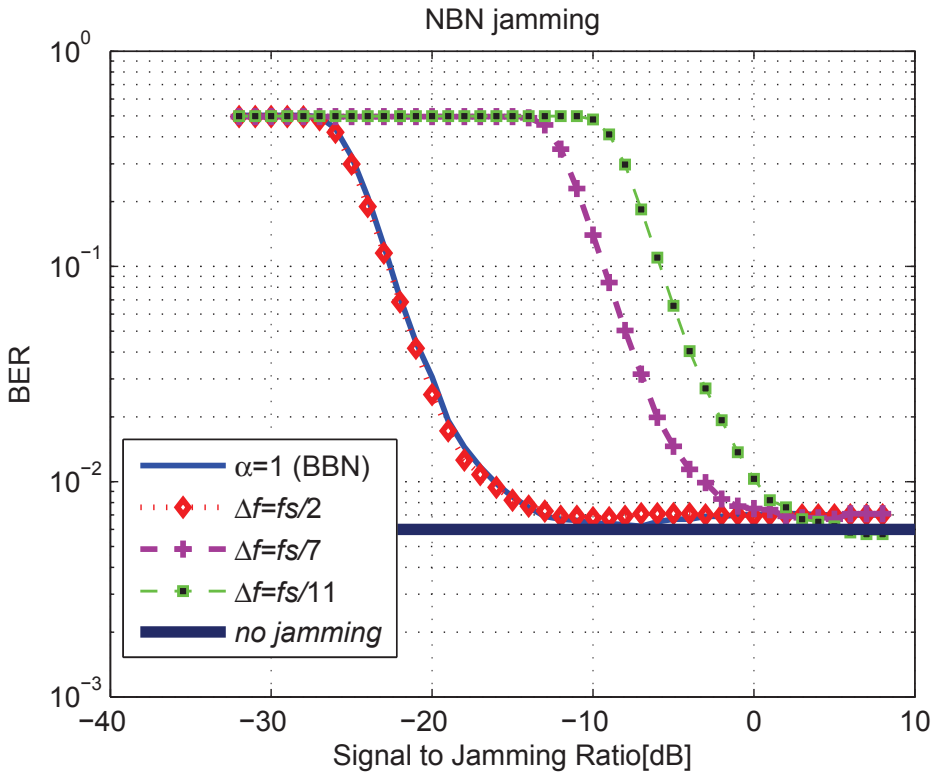

Figure 14: BER of FSK signal for NBN jamming for different Δ_f values.

3.2.3 Tone jamming

In tone jamming, one or more jammer tones are strategically placed in the spectrum. Where they are placed and their number affects the jamming performance. Two types of tone jamming are illustrated in Fig.11. As illustrated in Fig.11 (e), single-tone jamming places a single tone where it is needed. Estimation methods are used to detect the part of spectrum that is covered by adversary signals and based on that the proper jamming tone is selected. f_i represents this jamming tone. On the other hand, multiple-tone jamming distributes the jammer power among several tones. N specifies the number of tones that are used by the jammer signal to attack the adversary. Tone jammers are generally strong jammers because of their compact spectrum features. This type of jamming signals are less vulnerable to frequency hopping. To make this strategy feasible, perfect timing and phase match is very

essential to be satisfied. Fig.15 demonstrates the effect of tone jamming on the BER performance of FSK modulation assuming various tones. If jammer tone exactly matches that of the transmitted signal, $f/f_c = 1$, it means that the jammer uses its full capacity and is destroying the adversary signal. $f/f_c = 1$ is the ideal case from jammer's point of view in which there is perfect match between the carrier FSK signal and jamming signal's tones. This is a very strong jammer, however its implementation is difficult because of its compact spectrum nature. The effect of increasing the SJR is also explored in Fig.5 for$f/f_c = 300$, $f/f_c = 0.06$ and $f/f_c = 0.8$. The signal to jamming ratios required for achieving BER $10^{-2}$are -15.15 dB, 9.37 dB and 16.06 dB respectively. As the figure illustrates, as we get away from the perfect case, where the fraction is unity, the jammer's performance gets worse. The performance of BBN jamming is also plotted as a bench mark. For example $f/f_c = 300$ performs almost like BBN jamming. There is 1.4 dB, 31 dB, 25.95 dB and 14.5 dB difference in the required SNR for achieving BER of 10^{-2} for $f/f_c = 300$, $f/f_c = 1$, $f/f_c = 0.06$ and $f/f_c = 0.8$ respectively. Excluding the ideal case, where the ratio is unity, the second best jammer is $f/f_c = 0.8$. Assuming SNR = 8 dB, BER is 0.006 for the no jamming case which is depicted in the figure with a straight solid line as a bench mark.

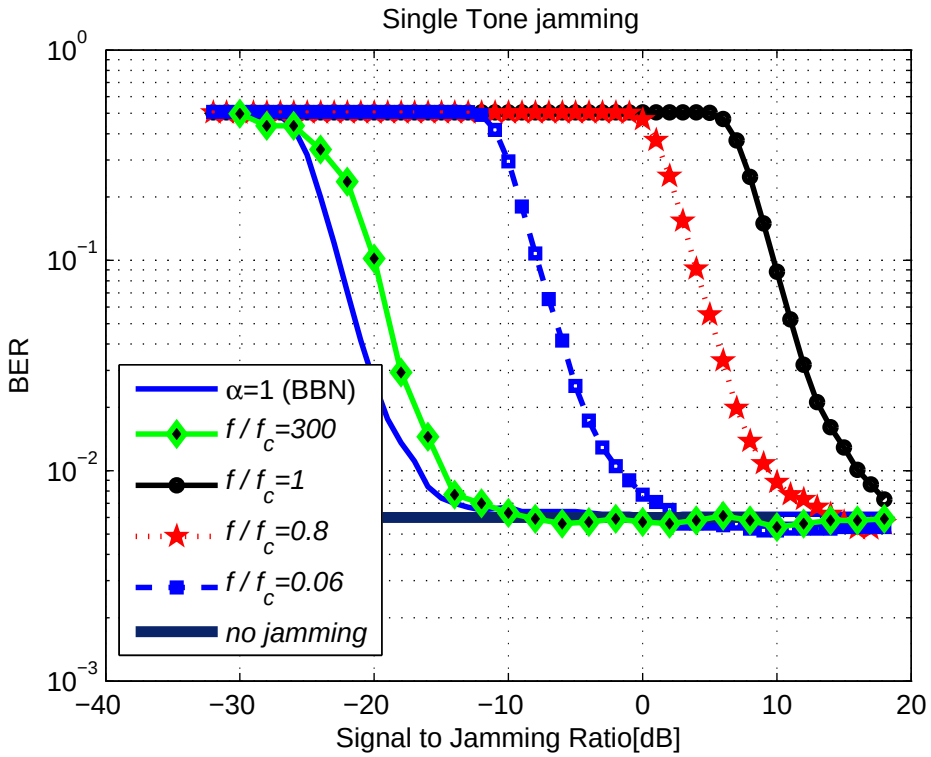

Figure 15: BER of signal with different set of tones for single tone jamming FSK and BBN.

Fig.16 evaluates performance of multi-tone jammer which highly depends on the number of jamming tones. As the number of tones increases the jammer gets stronger. The match of jamming tones and the transmit signal tone is also necessary. The effect of change is exactly the same as single tone jamming and that's why it is not plotted here. The intuition behind developing multi-tone jammers is to reinforce the jammer against FHSS systems in which the signals is frequently jumping form one hop to another and multi-tone jamming will increase the efficiency of the jamming. Assuming SNR = 8 dB, BER is 0.006 for the no jamming case which is depicted in the figure with a straight solid line as a bench mark.

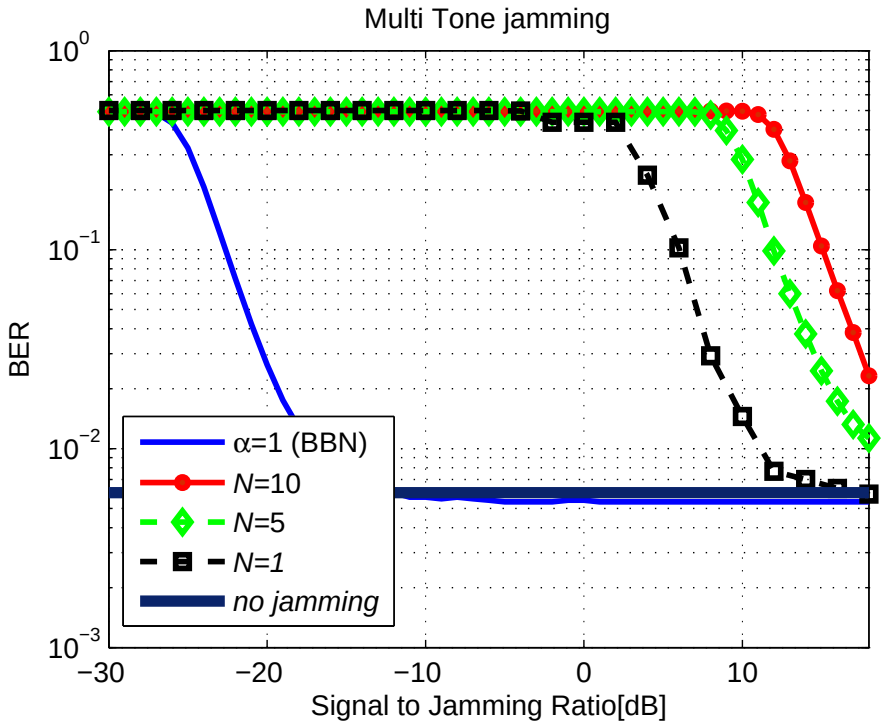

Figure 16: BER of signal with multi-tone jamming FSK and BBN.

So far we explored the jamming signals in frequency domain but, there is no limitation for designing the jamming signlas in this domain as discussed above. Swept Jamming, Pulse Jamming and Follower Jamming are other types of common jamming strategies that will be introduced brifly in the following.

Swept Jamming

A concept similar to broadband or partial-band noise jamming is swept jamming. This is when a relatively narrowband signal, which could be as narrow as a tone but more often is a PBN signal, is swept in time across the frequency band of interest. At any instant in time, the jammer is centered on a specific frequency and the only portion of the spectrum being jammed is in a narrow region around this frequency.

Pulse Jamming

Pulse jammer is the equivalent of PBN jamming in time domain. In other words the fraction is defined as the portion of time that the channel is covered by the jammer,

whereas for PBN jammer this parameters corresponds to the portion of frequency spectrum that is covered at a specific time.

Follower Jamming

A follower jammer attempts to locate the frequency to which the transmitter went, identify the signal which is targeted to attack, and jam at the new frequency. This jamming waveform could be in the form of tones or it could modulate the tones with, any suitable analog modulation type [31].

3.2.4 Jamming Parameters

The power of the jamming signal and frequency hopping (FH) related parameters are the main jamming parameters that effect its efficiency irrespective of the type of strategy. In the previous figures, we assume that SNR is fixed and we demonstrated the BER performance with respect to SJR. In Fig.17, we demonstrate BER with respect to SNR for different values of SJR. As the power of jamming increases (SJR decreases) the performance gets worse to the point that in jammer power 0 dB the total signals gets lost in the jammer. It is assumed that there is no FH jamming avoidance in this simulation and the jammer uses single tone type in order to attack the signal.

Frequency hopping technique has been widely used in tactical communications to avoid jamming strategies. In the systems that are equipped with FH the jammers prefer tone jamming to noise jamming. The intuition behind this preference is that it can be followed by follower strategies so that it would hit the targeted channel. Assuming single-tone jamming system, in Fig.18 the effect of FH-FSK signal is compared to the case that there is no FH in the single tone jamming effected system. The figure illustrates that FH can show significant degradation in performance of jamming signal. Increasing the number of hopping channels results in better BER for the FH-FSK system. Considering all the discussions above, single tone jamming

with perfect estimation of the FSK signal's characteristics, is the strongest strategy that an adversary can use.

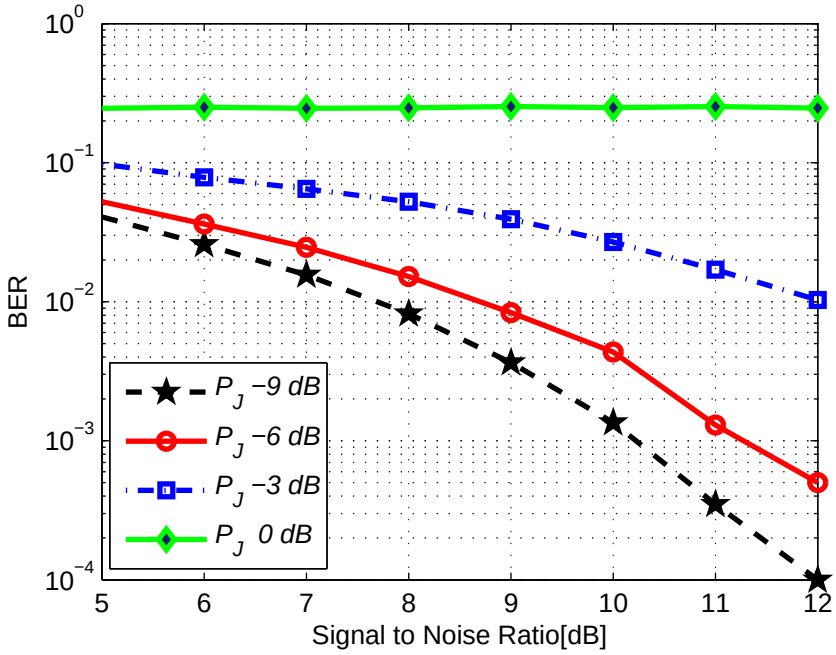

Figure 17: Single tone jamming signal power effect on BER of FSK system.

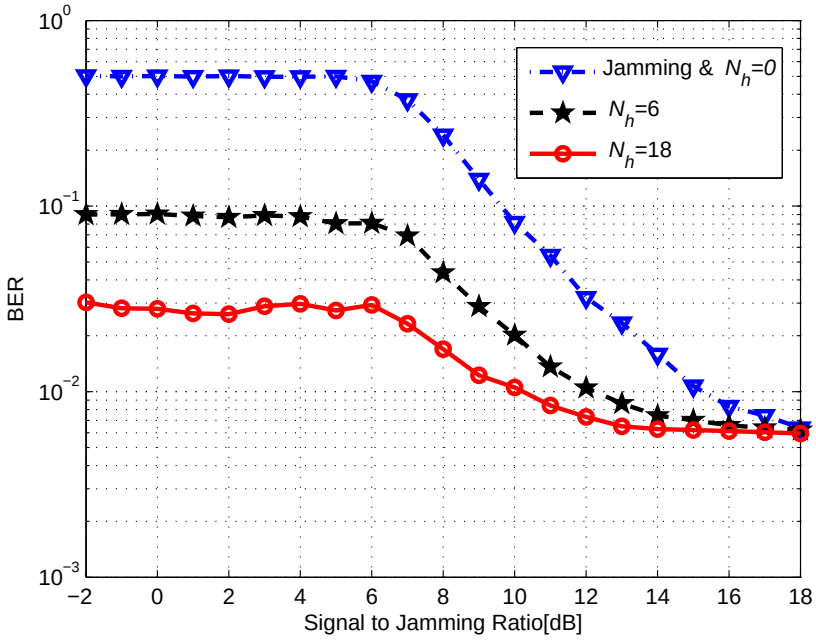

Figure 18: FH effect on single tone jamming attacked FSK system (for SNR = 8 dB)

3.3 Effect of Jamming Signals on LDPC-coded CPM systems

3.3.1 Broadband noise (BBN) jamming and Partial-band Noise (PBN) jamming

The same investigations are done in the following for an LDPC-coded CPM system. Starting from partial band noise (PBN) jamming signals, Fig.19 demonstrates the effect of PBN jamming on the BER performance of LDPC-coded CPM signal assuming various α values. The performance of BBN (which means PBN with $\alpha = 1$) is also included as a benchmark. The BER performance is plotted with respect to signal-to-jamming ratio (SJR) which is defined before. Here, we assume that SNR = 7.61 dB. It is observed that as α increases and approaches to one, the jamming effect gets weaker since the jamming energy is now spread over a wider spectrum. Assuming SNR = 7.61 dB, BER is 0.001 for no jamming case which is depicted in the figure with a straight solid line as a bench mark. It is also illustrated that for achieving BER = 10^{-2} for $\alpha = 1$, $\alpha = 0.5$, $\alpha = 0.3$ and $\alpha = 0.1$ the required SJRs are 3.6 dB, 10.61 dB, 11.62 dB and 12.87 dB respectively.

Fig.20 demonstrates the effect of non-continuous PBN jamming signal on the BER performance of LDPC-coded CPM modulation assuming various set of α values. These sets are chosen as they used to be for FSK modulation. Assuming SNR = 7.61 dB, BER is 0.001 for no jamming case which is depicted in Fig.20 with a straight solid line as a bench mark. It is also illustrated that for achieving BER = 10^{-2} for $\boldsymbol{\alpha_1}$, $\boldsymbol{\alpha_2}$ and $\boldsymbol{\alpha_3}$ the required SJRs are 14.39 dB, 15.94 dB and 18.78 dB respectively. It means that $\boldsymbol{\alpha_1}$ outperforms $\boldsymbol{\alpha_2}$ in terms of jamming effectiveness. In other words, BER of the system gets worse. Both $\boldsymbol{\alpha_1}$ and $\boldsymbol{\alpha_2}$ consist of three partial-band waveforms, but $\boldsymbol{\alpha_2}$ has a wider coverage in the spectrum. This results in a weaker jamming signal. Meanwhile $\boldsymbol{\alpha_3}$ shows the strongest jamming performance.

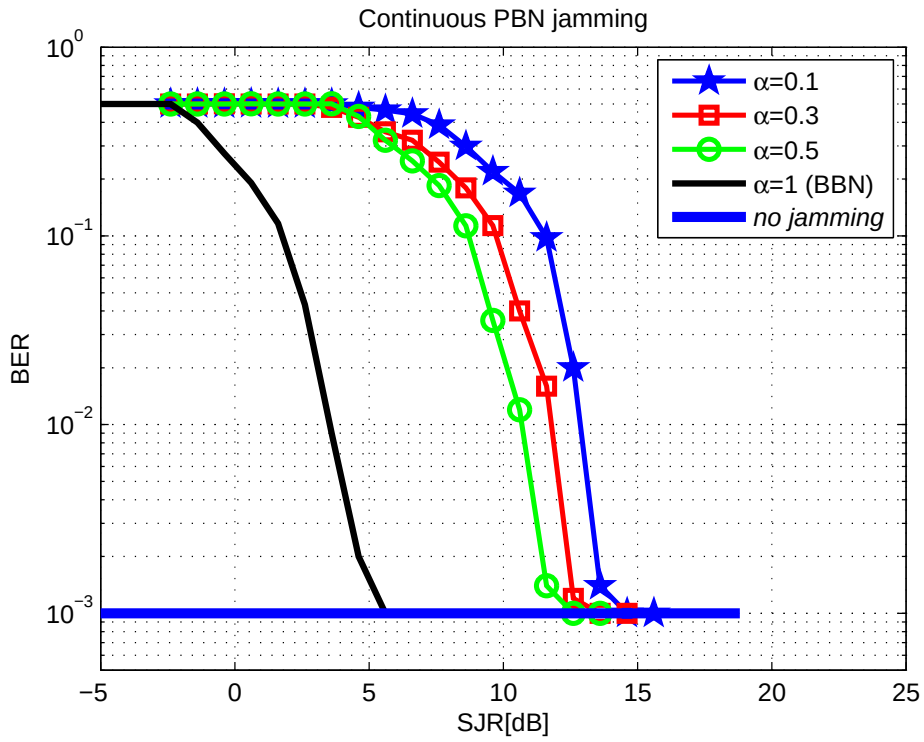

Figure 19: BER of LDPC-coded CPM for continuous PBN with different α values (SNR = 7.61 dB).

3.3.2 Narrowband noise (NBN) jamming

As it was mentioned in the beginning, Narrowband noise (NBN) jamming places all of the jamming energy into a single channel. The narrower the channels is the stronger the jammer performs. Assuming SNR = 7.61 dB, BER is 0.001 for the no jamming case which is depicted in Fig.21 with a straight solid line as a bench mark. It is also illustrated that for achieving BER = 10^{-2} for $\Delta f = f_s/3$ and $\Delta f = f_s/8$ the required SJRs are 5.78 dB and 7.61 dB respectively. As for the BBN jamming this value reduces to 3.6 dB which represents a weak jamming strategy. As the channel gets divided to narrower sub-channel the jammer gets stronger for instance, $\Delta f = f_s/8$ requires 4.01 dB more SJR than the BBN jamming for BER of 10^{-2} which shows significant improvement in jammer's performance and represents the strongest jammer in the figure.

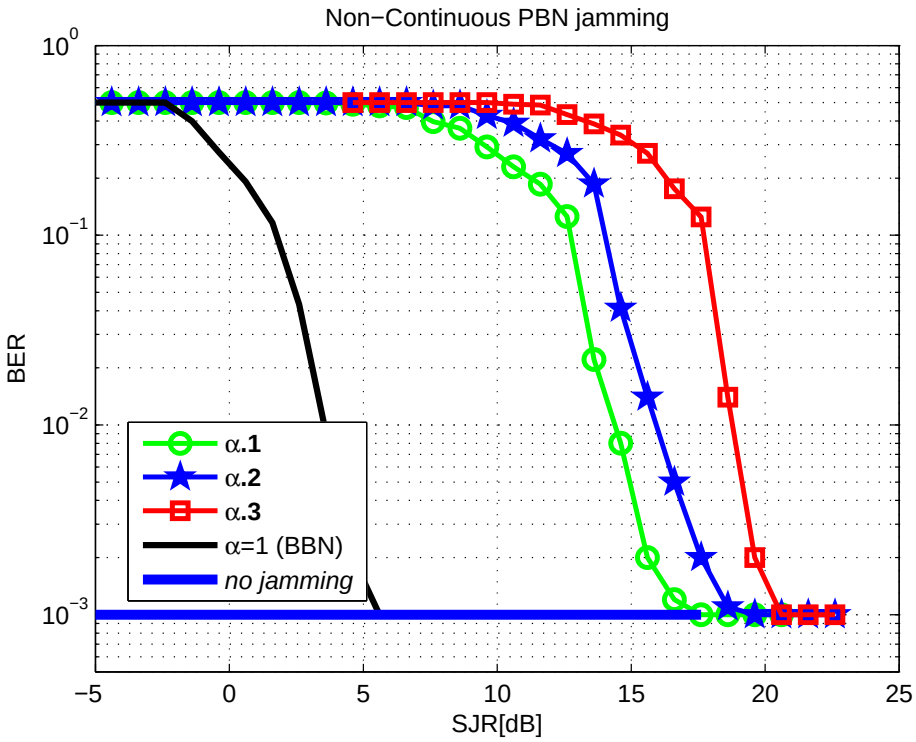

Figure 20: BER of LDPC-coded CPM for non-continuous PBN with different sets of α values (SNR = 7.61 dB).

3.3.3 Tone Jamming

Fig.22 demonstrates the effect of tone jamming on the BER performance of LDPC-coded CPM assuming various tones. If jammer tone exactly matches that of the transmitted signal, $f/f_c = 1$, it means that the jammer uses its full capacity and is destroying the adversary signal. This is a very strong jammer, however its implementation is difficult because of its compact spectrum nature. The effect of increasing the SJR is also explored in Fig.22 for $f/f_c = 1$, $f/f_c = 0.8$ and $f/f_c = 0.5$. The signal to jamming ratios required for achieving BER of 10^{-2} are 10.62 dB, 8.03 dB and 5.6 dB respectively. As the figure illustrates, as we get away from the perfect case where the fraction is unity, the jammer's performance gets worse. The performance of BBN jamming is also plotted as a bench mark. Excluding the ideal case, where the ratio is unity, the second best jammer is $f/f_c = 0.8$. Assuming SNR = 7.61 dB, BER is

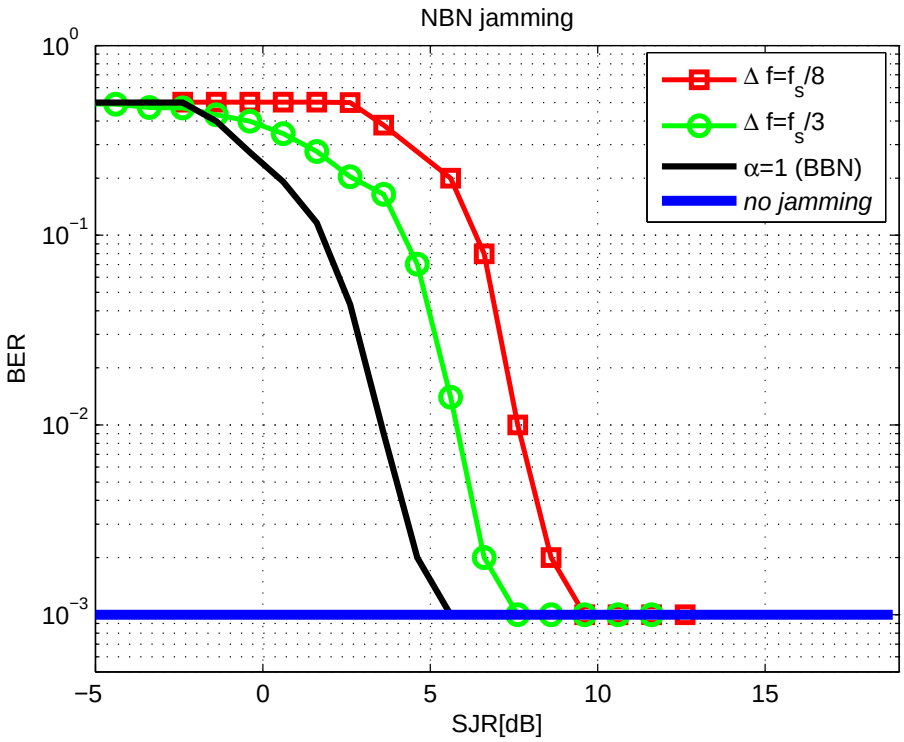

Figure 21: BER of LDPC-coded CPM signal for NBN jamming for different Δ_f values.

0.001 for the no jamming case which is depicted in the figure with a straight solid line as a bench mark.

Fig.23 evaluates performance of multi-tone jammer which highly depends on the number of jamming tones. N is representing the number of tones that are used for jamming. As the number of tones increases the jammer gets stronger. The phase match of jamming tones and the transmit signal tone is also necessary which has the same effects that are discussed in FSK modulated system. It is illustrated in Fig.23 that for $N = 10$, $N = 5$ and $N = 1$ SJRs of 11.9 dB, 10.6 dB and 7.6 dB are required correspondingly to achieve BER of 10^{-2}.

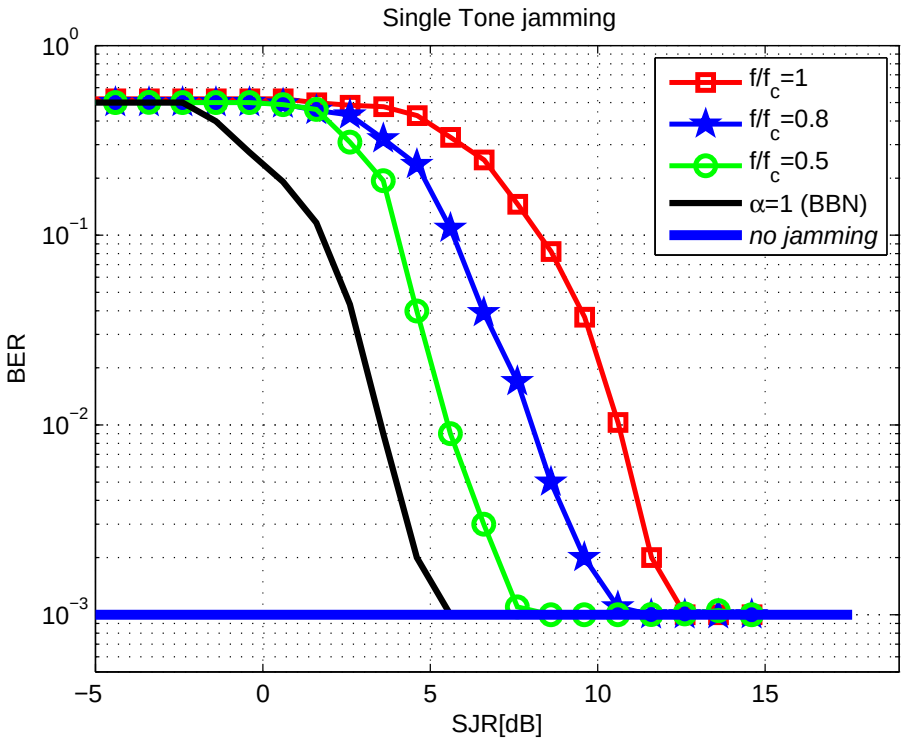

Figure 22: BER of signal with different set of tones for single tone jamming LDPC-coded CPM and BBN.

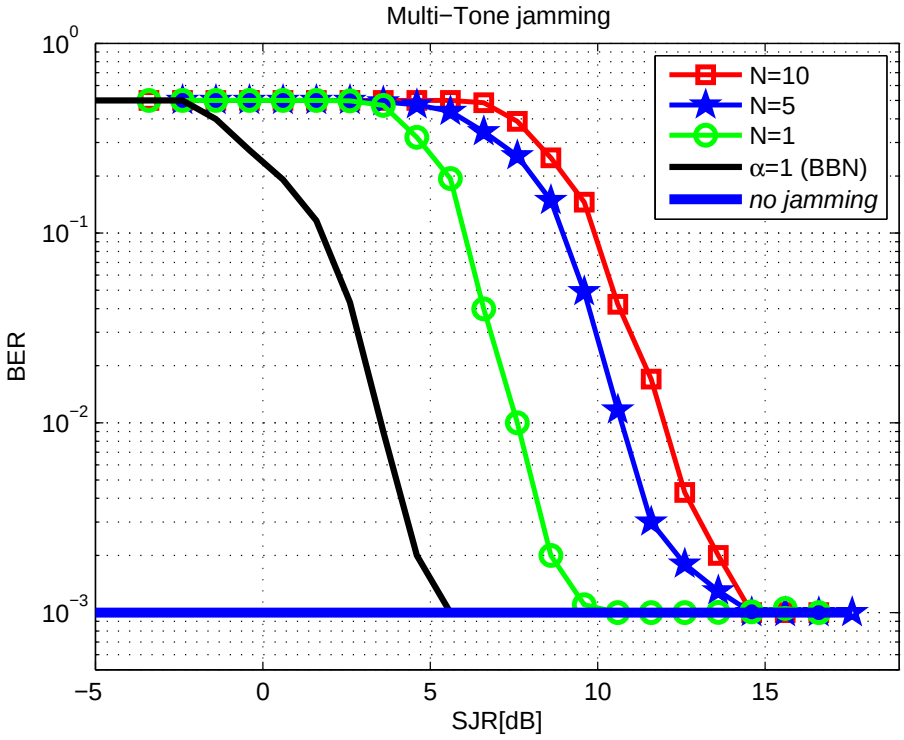

Figure 23: BER of signal with different set of tones for single tone jamming LDPC-coded CPM and BBN.

3.3.4 Jamming Parameters

In Fig.24 we are discussing the effect of single tone jamming signal on LDPC-coded CPM signal with $M = 4$, $L = 2$ and $h = 0.1$ which corresponds to best LDPC-coded CPM in terms of joint spectral and power efficiency as well as complexity. There are three different cases which are explored in this figure. The first case is representing the signal performance when there is no jamming which requires SNR of 7.61 dB for achieving BER of 10^{-3}. The next two curves are related to the FH equipped system which have 64 and 240 hopping channels (N_h). The former requires SNR of 8.15 dB for achieving SNR of 10^{-3} and the latter requires SNR of 7.93 dB for showing the same performance. As it was expected FH makes the system robust against jamming attacks. Increasing the number of hopping channels enhances this robustness which is illustrated in the figure as well. On the other hand, when there is no frequency hopping and the system is attacked by a single tone jamming signal, the performance degradation is so high that the communication is no longer reliable. This is represented by $N_h = 0$, where it is assumed that the jammer has perfect estimation of the location of the signal in the spectrum.

Fig.25 shows the effect of jamming power on BER of LDPC-coded CPM modulated system. As the power of jamming increases the performance gets worse to the point that in jammer with power of 0 dB the total signals gets lost in case the jammer hits the correct location of the signal. It is assumed that the system makes use of frequency hopping technique with 64 hopping channels and the jammer uses single tone strategy to attack the transceiver.

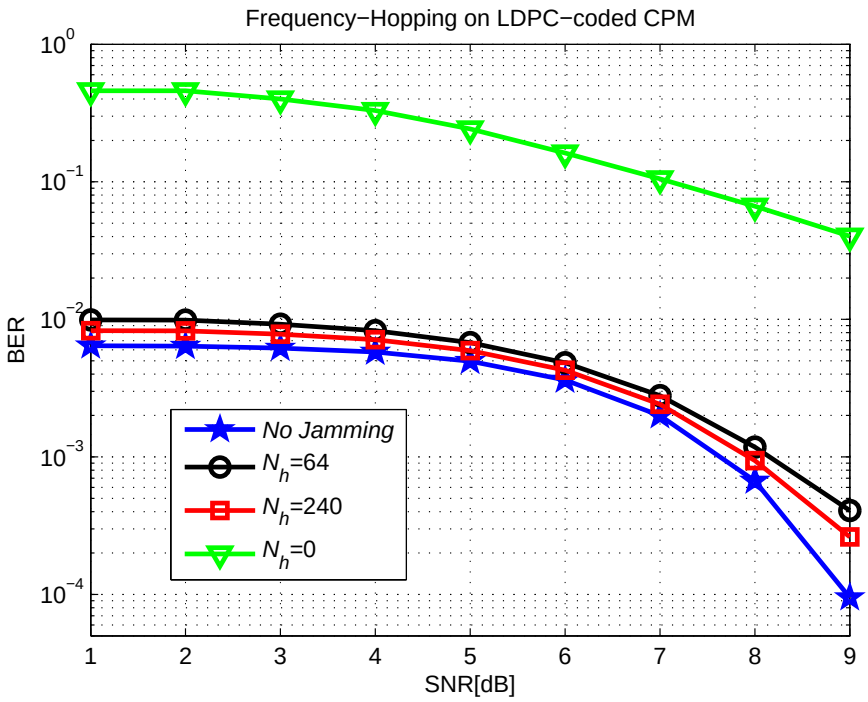

Figure 24: FH effect on single tone jammed LDPC-coded CPM (for SNR = 7.61 dB)

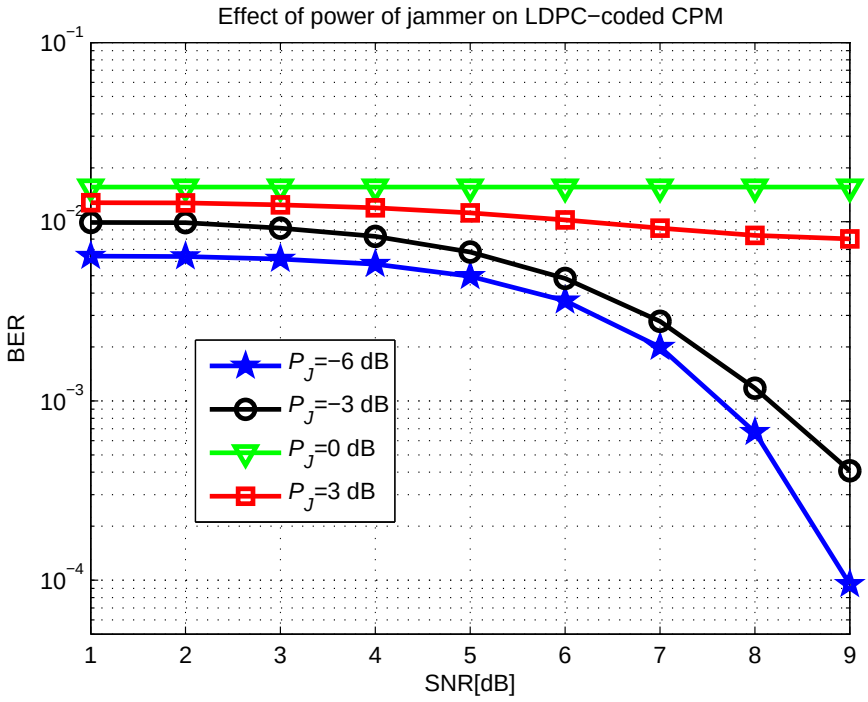

Figure 25: Effect of power of single-tone jamming signal on BER of LDPC-coded CPM system.

CHAPTER IV

CONCLUSION

In this thesis, with focus on tactical waveform design, we considered an LDPC-coded CPM system and investigated the proper choice of transmission parameters. High coding gain and significant spectral efficiency made the basis of this selection. The aforementioned parameters include modulation index, alphabet size, pulse shape duration and code rate. Utilizing a systematic search procedure, we identified the proper transmission parameters to achieve a targeted spectral efficiency and error rate under a constraint on demodulator complexity. $M = 4$, $L = 2$, $h = 0.1$ and $R = 0.75$ are the parameters of the scheme that was selected out of 270 possible schemes. Then we demonstrate the superior performance of selected LDPC-coded CPM scheme over its competitors. In context of military communications, jamming signals can be very detrimental for the system. Hence, we explored different types of jamming signals and their effect on the overall performance of the system. As a result of this investigation, single tone jamming with perfect estimation of the FSK signal's characteristics, was considered the strongest strategy that an adversary could use to attack an anti-jamming system. On the other hand, any communication system should take preventive measures against jamming attacks. Hence, in this thesis we utilized frequency hopping spread spectrum as a mean of protection against jamming and we discussed the effects of this technique's parameters on system's performance.

Bibliography

[1] A. P. Worthen and P. Wu, "CPM optimization for low-complexity serial concatenated CPM," in *Proc. IEEE Military Communications Conference(MILCOM)*, (Boston), Oct. 2003.

[2] N. Mazzali, G. Colavolpe, and S. Buzzi, "CPM-Based Spread Spectrum Systems for Multi-User Communications," *IEEE Trans. Wireless Commun.*, vol. 12, pp. 358–367, Jan. 2013.

[3] E. Casini, D. Fertonani, and G. Colavolpe, "Advanced CPM receiver for the NATO tactical narrowband waveform," in *Proc. IEEE Military Communications Conference(MILCOM)*, (San Jose,CA), Oct. 2010.

[4] C. Brown and P. Vigneron, "A reduced complexity iterative non-coherent CPM detector for frequency hopped wireless military communication systems," in *Proc. IEEE Military Communications Conference(MILCOM)*, (Atlantic City, NJ), Oct. 2005.

[5] J. Nieto and W. Furman, "Constant-amplitude waveform variations of US MIL-STD-188-110B and STANAG 4539," in *Proc. 10th IET International Conference on Ionospheric Radio Systems and Techniques (IRST)*, (Beijing, China), Jul. 2006.

[6] B. K. Levitt, U. Cheng, A. Polydoros, and M. K. Simon, "Optimum detection of slow frequency-hopped signals," *IEEE Trans. Commun.*, vol. 42, pp. 1990–2000, Feb. 1994.

[7] M. Xiao and T. M. Aulin, "On Analysis and Design of Low Density Generator Matrix Codes for Continuous Phase Modulation," *IEEE Trans. Wireless Commun.*, vol. 6, pp. 3440–3449, Sept. 2007.

[8] K. Narayanan, I. Altunbas, and R. Narayanaswami, "Design of serial concatenated MSK schemes based on density evolution," *IEEE Trans. Commun.*, vol. 51, pp. 1283–1295, Aug. 2003.

[9] C. Brown and P. Vigneron, "Spectrally Efficient CPM Waveforms for Narrowband Tactical Communications in Frequency Hopped Networks," in *Proc. IEEE Military Communications Conference(MILCOM)*, (Washington, DC), Oct. 2006.

[10] T. Tapp, R. Mickelson, R. Groshong, C. Behmlander, J. T. Graf, and J. C. Whited, "Turbo-detected coded continuous-phase modulation for military UHF satellite communications," in *Proc. IEEE Military Communications Conference(MILCOM)*, (Anaheim, CA), Oct. 2002.

[11] D. Hermes and F. Kragh, "A Bandwidth Efficient Constant Envelope Modulation with Reed-Solomon Coding," in *Proc. IEEE Pacific Rim Conference on*

Communications, Computers and Signal Processing (PacRim), (Victoria, BC), Aug. 2007.

[12] X. Rui, Z. Dan-feng, and Z. Tie-lin, "An Improved Method for the Convergence of Iterative Detection in Turbo-CPM System," in *Proc. IEEE 5th International Conference on Wireless Communications, Networking and Mobile Computing (WiCom)*, (Beijing, China), Sept. 2009.

[13] X. Rui, Z. Dan-feng, and X. Chun-li, "Power and bandwidth efficient LDPC coded CPM with iterative decoding," in *Proc. 12th IEEE International Conference on Communication Technology (ICCT)*, (Nanjing), Nov. 2010.

[14] S.-Y. Chung, J. Forney, G.D., T. Richardson, and R. Urbanke, "On the design of low-density parity-check codes within 0.0045 db of the Shannon limit," *IEEE Commun. Lett.*, vol. 5, pp. 58–60, Feb. 2001.

[15] J. Proakis and M. Salehi, *Digital Communications*. McGraw-Hill Education, New York, USA, 2007.

[16] H. R. Sadjadpour, "Maximum a posteriori decoding algorithms for turbo codes," in *AeroSense 2000*, pp. 73–83, International Society for Optics and Photonics, 2000.

[17] R. Gallager, "Low-density parity-check codes," *IRE Trans. Information Theory*, vol. 8, pp. 21–28, Jan. 1962.

[18] I. L. S. Committee *et al.*, "IEEE standard for local and metropolitan area networks part 16: Air interface for fixed and mobile broadband wireless access systems amendment 2: Physical and medium access control layers for combined fixed and mobile operation in licensed bands and corrigendum 1," *IEEE Std 802.16-2004/Cor 1-2005*, 2006.

[19] A. Shokrollahi, "LDPC codes: An introduction," in *Coding, cryptography and combinatorics*, pp. 85–110, Springer, 2004.

[20] Z. Wu, *Coding and iterative detection for magnetic recording channels*. Springer, 2000.

[21] F. Kschischang, B. Frey, and H.-A. Loeliger, "Factor graphs and the sum-product algorithm," *IEEE Trans. Information Theory*, vol. 47, pp. 498–519, Feb. 2001.

[22] T. K. Moon, "Error correction coding," *Mathematical Methods and Algorithms. Jhon Wiley and Son*, 2005.

[23] T. Moon, *Error Correction Coding: Mathematical Methods and Algorithms*. Wiley, New Jersey, USA, 2005.

[24] R. Poisel, *Modern Communications Jamming: Principles and Techniques*. Artech House, 2011.

[25] R. A. Poisel, "Modern communications jamming principles and techniques, artech house," *Inc., Norwood, MA*, 2011.

[26] K. Sripimanwat, *Turbo code applications*. Springer, Dordrecht, The Netherlands, 2005.

[27] J. B. Anderson, T. Aulin, and C.-E. Sundberg, *Digital phase modulation*. Springer, 1986.

[28] P. D. Welch, "The use of fast Fourier transform for the estimation of power spectra: A method based on time averaging over short, modified periodograms," *IEEE Trans. Audio Electroacoust.*, vol. 15, pp. 70–73, Jun. 1967.

[29] F. Amoroso, "Pulse and spectrum manipulation in the minimum/frequency/shift keying/msk/format," *IEEE Transactions on Communications*, vol. 24, pp. 381–384, 1976.

[30] T. Aulin, G. Lindell, and C.-E. Sundberg, "Selecting smoothing pulses for partial-response digital fm," in *IEE Proceedings F (Communications, Radar and Signal Processing)*, vol. 128, pp. 237–244, IET, 1981.

[31] D. Torrieri, *Principles of spread-spectrum communication systems*. Springer, 2011.

[32] K. Narayanan, I. Altunbas, and R. Narayanaswami, "On the design of LDPC codes for MSK," in *Proc. IEEE Global Telecommunications Conference (GLOBECOM)*, (San Antonio, TX), Nov. 2001.